SOUTHERN PLAINS
TRANSPORTATION CENTER

Monitoring Extreme Loading and Climate Impact on Infrastructure

Julie Ann Hartell, Ph.D.
Hang Zeng

SPTC14.2-09-F

Southern Plains Transportation Center
201 Stephenson Parkway, Suite 4200
The University of Oklahoma
Norman, Oklahoma 73019

DISCLAIMER

The contents of this report reflect the views of the authors, who are responsible for the facts and accuracy of the information presented herein. This document is disseminated under the sponsorship of the Department of Transportation University Transportation Centers Program, in the interest of information exchange. The U.S. Government assumes no liability for the contents or use thereof.

TECHNICAL REPORT DOCUMENTATION PAGE

1. REPORT NO.	2. GOVERNMENT ACCESSION NO.	3. RECIPIENTS CATALOG NO.
SPTC 14.2-09		

4. TITLE AND SUBTITLE	5. REPORT DATE
Monitoring Extreme Loading and Climate Impact on Infrastructure	October 30, 2018
	6. PERFORMING ORGANIZATION CODE
7. AUTHOR(S)	8. PERFORMING ORGANIZATION REPORT
Hartell, Julie Ann; Zeng, Hang	
9. PERFORMING ORGANIZATION NAME AND ADDRESS	10. WORK UNIT NO.
School of Civil and Environmental Engineering Oklahoma State University 207 Engineering South Stillwater, OK 74078	11. CONTRACT OR GRANT NO. DTRT13-G-UTC36
12. SPONSORING AGENCY NAME AND ADDRESS	13. TYPE OF REPORT AND PERIOD COVERED
Southern Plains Transportation Center 201 Stephenson Pkwy, Suite 4200 The University of Oklahoma Norman, OK 73019	Final October 2014 – September 2018
	14. SPONSORING AGENCY CODE

15. SUPPLEMENTARY NOTES
University Transportation Center

16. ABSTRACT
Nondestructive ultrasonic and acoustic emission (AE) evaluation techniques have been used worldwide to assess in-service infrastructure related problems. Numerous studies have demonstrated the applicability and versatility of the techniques to assess and to monitor damage initiation and evaluate its progression for various deterioration processes. To address the problem of climate impact and traffic overload on concrete infrastructure, the aim of this research study is to investigate evaluation and monitoring methods using technologies such as AE monitoring capable of qualifying material damage due to weathering and service condition. For this study, actual Oklahoma climate conditions are evaluated and not national standard conditions, which may not be relevant to local settings nor realistic of field encountered deterioration mechanisms. Cyclic high temperature exposure, cyclic freezing and thawing exposure and cyclic wetting and drying exposure are considered in this study. A total of five different test methods are compared herein to determine the efficacy and sensitivity of the techniques to determine damage initiation and its extent. Two destructive tests, compression and flexural testing are compared with two nondestructive methods, ultrasonic pulse velocity and resonant frequency. It was found that resonant frequency testing might be more sensitive to changes in microstructure caused by microcrack formation while flexural testing was the least effective. Still, all methods discerned (with varying sensitivity) a change in properties after 30 cycles of freeze-thaw exposure, 90 cycles of high temperature variance and 90 cycles of wet-dry exposures. Acoustic emission (AE) monitoring was performed during mechanical loading. A simple AE parameter-based evaluation confirmed that found from the destructive and nondestructive study. Therefore, the method was determined to be effective in discerning changes in material integrity if the member evaluated is subjected to varying levels of stress.

17. KEY WORDS	18. DISTRIBUTION STATEMENT
Concrete, Acoustic Emission Monitoring, Nondestructive Testing, Durability	No restrictions. This publication is available at www.sptc.org and from the NTIS.

19. SECURITY CLASSIF. (OF THIS REPORT)	20. SECURITY CLASSIF. (OF THIS PAGE)	21. NO. OF PAGES	22. PRICE
Unclassified	Unclassified	70 + Cover	

SI* (MODERN METRIC) CONVERSION FACTORS

APPROXIMATE CONVERSIONS TO SI UNITS

SYMBOL	WHEN YOU KNOW	MULTIPLY BY	TO FIND	SYMBOL
		LENGTH		
in	inches	25.4	millimeters	mm
ft	feet	0.305	meters	m
yd	yards	0.914	meters	m
mi	miles	1.61	kilometers	km
		AREA		
in^2	square inches	645.2	square millimeters	mm^2
ft^2	square feet	0.093	square meters	m^2
yd^2	square yard	0.836	square meters	m^2
ac	acres	0.405	hectares	ha
mi^2	square miles	2.59	square kilometers	km^2
		VOLUME		
fl oz	fluid ounces	29.57	milliliters	mL
gal	gallons	3.785	liters	L
ft^3	cubic feet	0.028	cubic meters	m^3
yd^3	cubic yards	0.765	cubic meters	m^3
		NOTE: volumes greater than 1000 L shall be shown in m^3		
		MASS		
oz	ounces	28.35	grams	g
lb	pounds	0.454	kilograms	kg
T	short tons (2000 lb)	0.907	megagrams (or "metric ton")	Mg (or "t")
		TEMPERATURE (exact degrees)		
^oF	Fahrenheit	5 (F-32)/9 or (F-32)/1.8	Celsius	^oC
		ILLUMINATION		
fc	foot-candles	10.76	lux	lx
fl	foot-Lamberts	3.426	candela/m^2	cd/m^2
		FORCE and PRESSURE or STRESS		
lbf	poundforce	4.45	newtons	N
lbf/in^2	poundforce per square inch	6.89	kilopascals	kPa

APPROXIMATE CONVERSIONS FROM SI UNITS

SYMBOL	WHEN YOU KNOW	MULTIPLY BY	TO FIND	SYMBOL
		LENGTH		
mm	millimeters	0.039	inches	in
m	meters	3.28	feet	ft
m	meters	1.09	yards	yd
km	kilometers	0.621	miles	mi
		AREA		
mm^2	square millimeters	0.0016	square inches	in^2
m^2	square meters	10.764	square feet	ft^2
m^2	square meters	1.195	square yards	yd^2
ha	hectares	2.47	acres	ac
km^2	square kilometers	0.386	square miles	mi^2
		VOLUME		
mL	milliliters	0.034	fluid ounces	fl oz
L	liters	0.264	gallons	gal
m^3	cubic meters	35.314	cubic feet	ft^3
m^3	cubic meters	1.307	cubic yards	yd^3
		MASS		
g	grams	0.035	ounces	oz
kg	kilograms	2.202	pounds	lb
Mg (or "t")	megagrams (or "metric ton")	1.103	short tons (2000 lb)	T
		TEMPERATURE (exact degrees)		
^oC	Celsius	1.8C+32	Fahrenheit	^oF
		ILLUMINATION		
lx	lux	0.0929	foot-candles	fc
cd/m^2	candela/m^2	0.2919	foot-Lamberts	fl
		FORCE and PRESSURE or STRESS		
N	newtons	0.225	poundforce	lbf
kPa	kilopascals	0.145	poundforce per square inch	lbf/in^2

*SI is the symbol for the International System of Units. Appropriate rounding should be made to comply with Section 4 of ASTM E380. (Revised March 2003)

ACKNOWLEDGEMENTS

The authors would like to thank the Southern Plains Transportation Center for providing funding to realize this research project. The authors would like to thank OSU research assistants Meher Mandavilli, Ignatius Vasant, Laine Peitzmeir and Reed Doss for their time and effort on this project.

MONITORING EXTREME LOADING AND CLIMATE IMPACT ON INFRASTRUCTURE

Final Report

October 2018

Julie Ann Hartell, Ph.D., Assistant Professor

Hang Zeng, Graduate Research Assistant

Southern Plains Transportation Center

201 Stephenson Pkwy, Suite 4200

The University of Oklahoma

Norman, OK 73019

TABLE OF CONTENTS

LIST OF FIGURES

LIST OF TABLES

EXECUTIVE SUMMARY

As transportation infrastructure age, implementation of preservation strategies becomes challenging due to cumulative combination of weathering and service loads. With respect to concrete structures, cyclic temperature extremes along with moisture changes within a structural element are known to cause a variety of degradation processes causing the material to prematurely fail. As for heavy traffic routing, repeated loading at design capacity is sufficient to alter the material's mechanical and durability performance. At these stress levels (40% to 60% of the ultimate stress), microcracks start to initiate within a cementitious matrix. The combination of the two damaging mechanisms only amplifies the rate at which the material deteriorates. Visual manifestations of such causal deterioration are often noticeable to the naked eye once the affected material has lost its structural integrity. In this case, the material can no longer meet intended service needs and costly replacement and/or maintenance are required. Here preemptive and adaptive condition assessment systems is key to keeping healthy infrastructure and extend their service life at minimal cost.

Nondestructive ultrasonic and acoustic emission (AE) evaluation techniques have been used worldwide to assess in-service infrastructure related problems. Numerous studies have demonstrated the applicability and versatility of the techniques to assess and to monitor damage initiation and evaluate its progression for various deterioration processes. To address the problem of climate impact and traffic overload on concrete infrastructure, the aim of this research study is to develop evaluation and monitoring guidelines using testing technologies such as AE monitoring capable of qualifying material damage.

Here, actual Oklahoma climate conditions are evaluated and not national standard conditions, which may not be relevant to local settings nor realistic of encountered deterioration mechanisms. Cyclic high temperature exposure, cyclic freezing and thawing exposure and cyclic wetting and drying exposure are considered in this study.

A total of five different test methods are compared herein to determine the efficacy and sensitivity of the techniques to determine damage initiation and its extent. Two destructive tests, compression and flexural testing are compared with two nondestructive methods, ultrasonic pulse velocity and resonant frequency. It was found that resonant frequency testing might be more sensitive to changes in microstructure caused by microcrack formation while flexural testing was the least effective. Still, all methods discerned (with varying sensitivity) a change in properties after 30 cycles of freeze-thaw exposure and 90 cycles of high temperature variance and wet-dry cycles. Acoustic emission (AE) monitoring was performed during mechanical loading. A simple AE parameter-based evaluation confirmed that found for the destructive and nondestructive study. Therefore, the method was determined to be effective in discerning changes in material integrity if the sample is subjected to varying levels of stress.

1. INTRODUCTION

From their construction until the end of their service life, all infrastructures must endure the aging effects of weathering and loading. In the case of concrete structures, extreme temperature changes and overloading are known to cause micro-damage, which reduces the material's capability to withstand design loads. [1] Material degradation mechanisms are difficult to detect and assess as they initiate and cumulate. Typical condition assessment campaigns involve mobilizing personnel to conduct cumbersome, lengthy visual inspections and take multiple samples (e.g. cores) in areas manifesting problems, which offer limited information about the overall condition of the structure. In other words, they are costly and not very efficient. Moreover, when visual signs of material degradation start manifesting, the problem is often widespread and costly rehabilitation measures are necessary to maintain serviceability. Here, advanced monitoring tools are beneficial as they can assess the overall condition of a structure rapidly and continuously without compromising the integrity of the structure. The data gathered from such monitoring technologies can be transmitted via wireless networks and provide asset managers real-time information about the material's and structure's performance. Here, no personnel mobilization and no traffic disruption are required. In addition, if a serviceability problem arise, correct actions may be taken immediately and target the affected area only (not the whole structure).

To address the problematic, the project elaborated here forth proposes to develop evaluation and monitoring guidelines using ultrasonic evaluation and acoustic emission monitoring as the primary sensing technologies to assess the impact of weather and overloading on infrastructure thus maintaining transportation infrastructure in a "state of good repair". The implementation of such technologies require specialized skillsets but once in place, are easy to operate and maintain by stakeholders.

Therefore, to address the problem of climate impact and traffic overload on concrete infrastructure, the aim of this research study is to develop evaluation and monitoring

guidelines using sensing technologies such as AE monitoring capable of qualifying and quantifying material damage and locating zones in distress. First, critical infrastructure regions of Oklahoma were evaluated using climatological data for Oklahoma. This helped in determining the experimental exposure conditions which the concrete samples will be subjected to. These are based on critical temperature and humidity ranges along with their number of cycles per annum. Therefore, actual Oklahoma climate conditions were evaluated and not national standard conditions that may not be relevant to local settings nor realistic of encountered deterioration mechanisms. Moreover, the exposure conditions incorporate various levels of loading conditions to simulate material overload and cyclic deterioration at design loads. The effects of both exposure combinations on concrete properties were monitored and analyzed using AE and ultrasonic techniques. In turn, the gathered information will contribute towards developing guidelines the transportation industry can use so that infrastructure problems can be corrected sooner. This will result in improved public safety and reduced maintenance costs. The goals of this study are to:

- Improve our understanding of concrete degradation processes specific to Oklahoman weather conditions and how they may be assessed in service.
- Identify new evaluation tools and improve current guidelines for early onset detection, damage assessment and damage evolution caused by various climatic conditions.

This will be achieved through the following research objectives:

- Develop climatological profiles for critical freight transportation regions in Oklahoma and reproduce the exposure parameters in a laboratory environment.
- Qualify and quantify damage accumulation a concrete material as sustained under the developed weathering and loading conditions relevant to Oklahoma; and, evaluate its residual performance using primarily acoustic emission and ultrasonic methods.

2. LITERATURE REVIEW

A multitude of mechanism contribute to the deterioration of concrete materials in service. It is well known that from the beginning proper mixture design and construction practices are key to maximize durability and serviceability overtime. However, degradation related to service conditions is inevitable. Even if all provisions are met, all infrastructure will be subjected to some form of stress, e.g. from passing vehicles or extreme temperature differences. Microcracking will initiate and propagate under repeated action of such stresses; and, the initial material characteristics will be altered. [1] Visual manifestations of such causal deterioration are often noticeable to the naked eye once the affected material has lost its structural integrity. In this case, the material can no longer meet intended service needs and costly replacement and/or maintenance are required. Here preemptive and adaptive condition assessment systems is key to keeping healthy infrastructure and extend their service life at minimal cost. To accomplish such, the first step is to determine the present condition of the structure with respect to its environment and, then, monitor for changes in material characteristics and structural behavior. The following sections provide background information on condition assessment basics, which may be implemented and/or adapted by agencies along with an overview of technologies for monitoring and assessing material and structural integrity.

2.1 CONDITION ASSESSMENT OF INFRASTRUCTURE

In 1960's, the collapse of the Silver Bridge, which carried U.S. route 35 over Ohio River, aroused the recognition of the aging problem of bridges and interest in the requirement of periodic and consistent bridge inspection and maintenance [2]. In response of this tragedy, the first nationwide standard, National Bridge Investigation Standards (NBIS), was established in the 1970's by the Federal Highway Administration (FHWA) and American Association of State Highway and Transportation Officials (AASTHO) to assure the safety and maintenance quality of existing bridge structures. Three manuals,

AASTHO's *Manual for Maintenance Inspection of Bridges*, FHWA's *Bridge Inspector's Training Manual 70* and *Recording and Coding Guide for the Structure Inventory and Appraisal of the Nation's Bridges,* were subsequently developed and contributed to the early success of NBIS. Decades into its development, today's NBIS provides nationwide guidelines and policies regarding inspection procedures, frequency of inspections, qualification of personnel, identifying which bridge need to be inspected, defining the information to be collected and reported during the process of inspection. In nature, the field inspection format generally involves a visual condition survey of the structure that may include basic testing and sampling of materials. Meanwhile, detailed bridge inspection files including load rating, flood history, relative maintenance data and inspection reports are stored in the National Bridge Inventory. It is administered by FHWA and can be used to track bridge conditions, monitor compliance of NBIS and prioritize funding decisions. [3-4]

Based on *Manual for Bridge Evaluation,* the NBIS categorizes investigations types into seven classes: initial inspections, routine inspections, damage inspections, in-depth inspections, fractural-critical inspections, underwater inspections and special inspections. Among them, fracture-critical inspection is generally applied for steel bridges and underwater inspection focuses on the substructures and surrounding channels. Both inspection methods are out of scope for this project and will not be addressed herein. The definition or the goal of different types of inspection in NBIS are listed below [5]:

- Initial inspection is the first inspection of bridge, which aims at providing *Structure Inventory & Appraisal* data and other relevant information, determining the baseline of structure and identifying the potential problems and its corresponding locations of the inspected bridge.
- Routine inspection is the most used inspection method on bridge, which defines as the 'regularly scheduled inspections consisting of observations, measurements, or both, needed to determine the physical and functional condition of the bridge, to identify any changes from initial or previously recorded

conditions, and to ensure that structure continues to satisfy present service requirements.

- Damage inspection aims at assessing the extent of structural damage, determining the need for restriction or closure of the bridge and assessing the level of effort necessary to effect a repair.
- In-Depth Inspection has the goal of identifying the susceptible structural deficiencies that are not detected in routine inspections. So special inspection techniques, such as load rating and other more sophisticated nondestructive testing methods (ultrasonic pulse velocity, ground penetrating radar, half-cell potential, etc.), can be used to assist in determining the nature and/or extent of structural damage.
- Special inspection is typically to monitor the condition or the change in suspected structural deficiency over time.

More specifically for concrete structures, the American Concrete Institute (ACI) has similar procedures for assessing the condition of concrete structures, ACI 364 *Guide for Evaluation of Concrete Structures before Rehabilitation*. Here, the guide provides information pertaining to conducting two types of investigations: preliminary and detailed. A preliminary investigation generally involves gathering information about the structure documents and performing a visual condition survey. It gives the inspector a general idea about the location, extent and nature of distress features on a given structure for analysis of its condition. As is mentioned above, the goals or the scope of a preliminary investigation are similar with that of an initial inspection, routine inspection and damage inspection as per NBIS description. When a preliminary investigation is insufficient to determine the condition of a structure, a detailed investigation (as per ACI 364) or in-depth investigation (as per NBIS) may be necessary. It encompasses all steps of a preliminary investigation with, most importantly, a detailed test program that may involve sophisticated laboratory and field test schemes to determine material properties and structural behavior. [6]

Elaborating a test program may at times be challenging. A successful test program maximizes the level of pertinent information gathered at the lowest cost to the client. Here, accessibility to the structure, equipment and supplies required, duration of the test and level of expertise required to conduct the test and to interpret are all factors that will affect cost and feasibility of a program. Therefore, understanding underlying principles of testing and monitoring methods along with their degree in reliability and limitations are crucial to proper elaboration of a testing and monitoring program. [7]

2.2 OVERVIEW OF MONITORING METHODS

Table 2-1 provides basic information on monitoring techniques of structural behaviors, material properties, exposure parameters and common distress features encountered for concrete structures. The table provides a summary on the measurement principle and information provided; reliability and accuracy of the measurement; time to execute the measurement; relative cost of sensor and ancillary equipment; and, common advantages of the monitoring method.

2.3 ACOUSTIC EMISSION MONITORING

As seen in Table 2-1, there are many advantages to using acoustic emissions (AE) as a monitoring technique as it may provide various levels of information about the structural and material integrity irrespective of the ongoing problematic. As such, its potential for evaluating damage related to extreme weathering and loading is of interests for this study. AE is a well-known passive nondestructive evaluation technique with a high sensibility to flaw detection within an element as it is generated and progresses. The theoretical principles behind the AE method is that an internal displacement of material (e.g. dislocation of atoms, microstructure strain, micro-cracking) will generate a stress-pulse that will propagate through the material at a given speed from its initial location (event location) towards the surface boundaries of the element. AE sensors placed at the surface of the element can detect the minute pulse as it arrives at its surface. [8]

Table 2-1: Summary of sensors commonly used for monitoring

Test Method	Measurement	Level of Information	Accuracy	Reliability	Time of Test	Cost	Advantage
Electrical Resistivity	Electrical current flow	Corrosion risk	Middle	Middle	Fast	Low	Low cost and simple principle
Embedded Reference Electrode	Voltage difference between two electrodes	Chloride concentration, pH value and oxygen content	Middle	Middle	Real-time monitoring	Low	chemical stability in aggressive environment
Microelectromechanical systems	Shear stress between film and micro cantilever beam; Temperature of absorbed water molecule	Relative humidity and temperature	High	High	Real-time monitoring	Low	Small size sensors, could be embedded inside of concrete structure
Acoustic emission	Elastic wave vibrations in terms of electric signal	Damage evaluation, crack location and classification	High	Middle	Real-time monitoring	High	Non-destructive test; high sensitivity and passive nature
Fiber Bragg grating sensor	Shift of center wavelength	Strain	High	High	Real-time monitoring	High	Multiplexing capacity (strain, temperature or acceleration)
Vibrating wire sensor	Fundamental frequency of tensioned wire	Strain	High	High	Real-time monitoring	Low	Ease of attachment, robustness and accuracy
Digital image correlation	Picture element	Strain and displacement	High	High	Real-time monitoring	High	Non-contact full-field displacement measurement up to failure
LVDT	Change in magnetic flux inducing an AC voltage	Displacement	High	High	Real-time monitoring	Low	High degree of robustness, high resolution
Crackmeters	Change in resonant frequency of wire	Movement of crack surface	High	High	Fast	Low	Simple installation, high accuracy and low cost
Accelerometers	Voltage change by piezoelectric effect	acceleration force	High	High	Fast	Low	Low cost and robust

Acoustic emission (AE) is a well-known passive nondestructive evaluation technique with a high sensibility to flaw detection within an element as it is generated and progresses. The theoretical principles behind the AE method is that an internal displacement of material (e.g. dislocation of atoms, microstructure strain, micro-cracking) will generate a stress-pulse that will propagate through the material at a given speed from its initial location (event location) towards the surface boundaries of the element. AE sensors placed at the surface of the element can detect the minute pulse as it arrives at its surface. [8]

German scientist Joseph Kaiser discovered, in the early 1950s, that acoustic waves could be generated if the stress exceeded its previous maximum load level when he conducted tensile test on metal with cyclic loading process, which is named the 'Kaiser effect'. [9] This initiated research on acoustic emission for different materials and industrial applications. Specific to concrete, AE has been considered a reliable nondestructive technique either to assess the damage degree of concrete material under different durability mechanisms or to perform structural health monitoring on real structures with development of the research over last few decades.

For example, Kawasaki et al. investigated the corrosion process of reinforced concrete under wet-dry cycles with the aid of acoustic emission monitoring. Two stages of the corrosion process were evaluated: onset of corrosion and the corrosion induced cracks. The corrosion processes were confirmed by analysis of AE parameters, RA value, average frequency value and b value analysis. The decrease of RA value and increase of average frequency value are indication of the transition from tension cracks at the first stage to shear and mixed mode cracks at the second stage. Meanwhile, bigger fluctuations during the second stage of the corrosion process were observed, which implied that cracks were repeatedly generated during both stages in the corrosion process. [10]

Abdelrahman et al. used acoustic emission to monitor the alkali silica reaction (ASR) in concrete. The correlation between AE cumulative signal strength (CSS) and the length

change of specimen were demonstrated from their experiment. Meanwhile, AE intensity analysis was used to quantify the ASR damage degree of the specimens under different exposure durations. Also, two parameters, historical index and severity, have been successfully correlated with damage rating index (DRI) obtained from petrographic analysis. [11]

Qian et al. examined mortar samples pre-saturated with different concentrations of NaCl solution (0%, 0.7%, 3%, 10% and 23%) under different freeze-thaw cycles. All the samples except the one pre-saturated in 23% NaCl solution experienced a large number of AE events during the freezing period, which may result from damage induced by the hydraulic pressure from formation of ice. On the contrary, the sample pre-saturated in 23% NaCl solution had few AE events due to the fact that the lowest temperature setup in their experimental was higher than the eutectoid temperature of NaCl solution (the transition temperature from liquid to solid phase) [12].

In all case, AE monitoring aided in better understanding the durability mechanism, how they progressed and the potential level of damage sustained by the material affecting its integrity. As such, the following sections provides further information on the technique.

2.3.1 AE equipment and measurement

Generally speaking, AE equipment can be classified as the following categories based on the function it serves as part of an AE system: detection, amplification, filtering, display and analysis of signal. As seen in Figure 2-1, an AE transducer placed on the surface of the monitored element can detect incoming elastic waves (i.e. stress-pulse) which are generated from within the element by the material. Next, the received elastic wave is converted into an electrical signal that is amplified by a pre-amplifier and main amplifier. The signal can be filtered by band-pass filters to eliminate undesirable AE signals that lie outside the frequency range of interest. Finally, the filtered and amplified signal are stored in the AE computer for visualization and further data processing. [8]

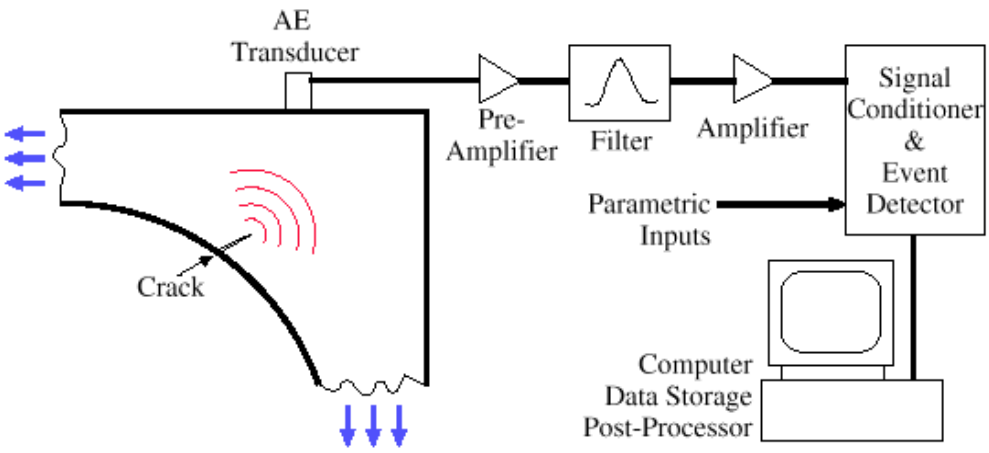

Figure 2-1: Typical schematic diagram of AE system. [13]

When selecting sensors for specific monitoring purposes, reliability of measurement and cost are two important parameters to consider. The sensor type will depend on the effective frequency range of elastic waves traveling through the given material medium and potential environing disturbances that may affect the detection of an AE event. As for economical factor, proper sensor placement and configuration to maximize signal detection and its strength at its reception will permit using a smaller number of sensors. Piezoelectric transducers, which can convert the surface displacement generated by a stress-pulse into an electrical signal (typically transforming 10^{-9} mm amplitude vibration to 10^{-6}V amplitude of electrical signal), are often used as AE sensors for signal detection. There are different types of AE sensors based on their effective frequency working range. Wide-band transducers can effectively capture a wider range of pulse frequencies but with less sensitivity; whereas, narrow-band transducers have a higher sensitivity but for a specific and smaller frequency range. The latter is generally preferable to use in practical applications because it can eliminate environing noise and thus increase the signal-to-noise ratio. [8]

For concrete materials, acoustic emission signals span a frequency range from several thousand hertz (kHz) up to 2 megahertz (MHz). For transducers of low frequency ranges (below 50 kHz), it may be difficult to differentiate environing noise from true AE events; on the other hand, pulse attenuation as it travels through the material becomes

an issue when utilizing transducers of high frequency range (between 50 kHz and 2 MHz). As such, concrete is a challenging material to monitor due to its heterogeneous nature. Therefore, it is of importance to properly assess potential environmental disturbance that may affect a measurement and to properly configure sensor placement to maximize signal strength at its reception. Here, filtering techniques and post-processing of data may also help to eliminate noise and maximize information from true AE signals [14].

Usually, the source signal in AE measurement is so weak that amplification of signal is required in order to record and analyze the signal. The gain of amplification can be expressed in dB (decibels) as the following expression.

$$\mathrm{dB} = 20log_{10}\left(\frac{E_o}{E_i}\right) \qquad \text{Eq. 2-1}$$

Where, E_o and E_i are output and reference input voltage of the signal, respectively. E_i is often set at 1μV at the sensor. For concrete materials, typically, the gain in pre-amplifier is in the range of 40 to 60 dB and the main amplifier has an additional gain of 20 to 60 dB. [10,14]

2.3.2 Acoustic Emission Parameters

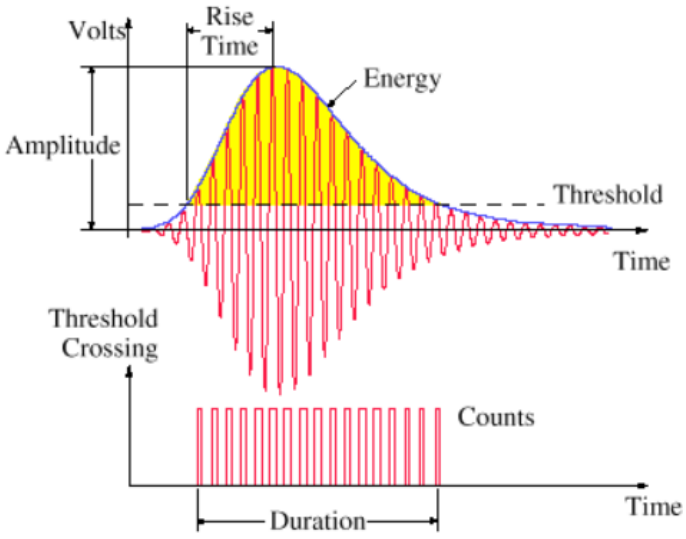

Figure 2-2: Schematic representation of AE waveform with parameters identified. [13]

There are two basic types of acoustic emission signals: continuous emission and burst emission (Figure 2-2). The former one is characterized by sustained signal level at relatively low amplitude level; while the latter one, on the contrary, is represented as a high amplitude event with relatively short duration times. It should also be noted that burst emission types often occur in cementitious material as internal damage initiate and propagate.

Hit is the terminology used for an AE signal or waveform recorded by an AE sensor. From this waveform, conventional AE parameters (e.g. amplitude, duration, energy) can be extracted. Other parameters, such as rise time and average frequency, are derived by mathematical operations of basic AE parameters. In the end, these AE parameters can be used to interpret changes in physical properties of the monitored material. [8] Followings are a few definitions for some fundamental AE parameters [15]:

- Hit: the signal that exceeds the pre-set threshold level within specific length of time and then it is record by AE system.
- Event: an occurrence of a local material change or mechanical action resulting in acoustic emission. An AE event could generate multiple AE hits received by one or more sensors.
- Count: the number of times which AE signals exceed the threshold level within any given time range.
- Amplitude: the peak voltage of a given event. It should be noted that the amplitude here should be understood as the sensor response after propagating in the material and attenuation rather than the amplitude of AE source itself.
- Rise time: the time interval between the initial time of AE signal above threshold level and the time of peak amplitude is reached.
- Duration: the time interval between the initial time of AE signal above threshold level and the time of last AE count in an AE event.
- Energy: defines as the area under AE signal or rectified signal envelope in time domain, which is sensitive to AE parameter amplitude and duration.
- Average frequency: it is calculated from “AE count” divided by “duration”.
- RA values: it is calculated from “rise time” divided by “amplitude”.

- Frequency centroid: it represents the weighted frequency value and can be correlated with the ‘brightness’ of sound (wiki), which calculated from the sum of magnitude times frequency value over the sum of magnitude.
- Peak frequency: it defines as the point in the frequency domain that has maximum amplitude value.

2.3.3 Types of Acoustic Emission Analysis Techniques

There are two major categories regarding analysis techniques of AE data: parameter-based analysis and signal-based analysis. In the former one, AE parameters are extracted from actual AE signals whereas AE signals themselves are not recorded. In the past, AE systems could not handle large amounts of high frequency data due to the limitation of basic electronic components. So, parameter based analysis, which reduced complex waveform to a few parameters, was preferable at the time. Today, the high data recording speed and relatively less data storage space of parameter-based analysis makes it economical and efficient. But, difficulty in distinguishing AE events from noise when signal is simplified to different parameters is a disadvantage of this classical AE analysis technique. However, signal-based analysis provides better performance on signal and noise discrimination for the recorded signals that offers better results interpretation. [16] Now with improved computer and sensing technology such as increased data storage, development of waveform analysis hardware and data processing software, the current trend in AE testing transfers from parameter-based analysis to signal-based analysis. Thus signal-based analysis (Quantitative analysis), such as 3-D source localization, visualization, frequency analysis technique and moment tensor inversion, begin to draw researchers’ more attention. [8,14]

3. EXPERIMENTAL PROGRAM

The experimental methodology used herein is based on the development of weather profiles for the region of Oklahoma City, OK, to identify relevant weathering conditions that may be detrimental to concrete properties. Each weathering regimen were replicated in a laboratory environment where concrete samples were subjected to for a determined period of time. Acoustic emission and ultrasonic methods were utilized to assess the extent of damage accumulation sustained under the various weathering and potential loading conditions reminiscent of service conditions in the field. The following sub-sections elaborate on the experimental approach devised to accomplish the objectives of the proposed project.

3.1 CLIMATOLOGICAL SURVEY

Due to the impact of temperature and moisture variations on concrete leading to material distress, three different exposure regimens based on weathering extremes were evaluated: cyclic freezing and thawing (F-T), high temperature variations (H-T) and cyclic wetting and drying simulating precipitations (W-D). To define exposure parameters, climate conditions in Oklahoma were evaluated rather than national standard conditions, which may not be relevant to local settings nor realistic of encountered deterioration mechanisms within the state. The developed criteria were based on critical temperature and humidity data recorded by environmental monitoring stations providing mesoscale weather data for a specific region. Regions of interest were targeted based on permitted heavy-load traffic routes and presence of bridge infrastructure.

It was determined that Oklahoma City was a region of interest due to its degree in temperature variability and critical infrastructure system. A statistical analysis was performed to outline the exposure regimen criteria for the three series of exposure regimens. The relevant temperature and humidity profiles for determining the sample

exposure regimens were developed using historical climatological data for a ten-year period, 2004 to 2014, which was obtained from the National Oceanic and Atmospheric Administration (NOAA) database for Oklahoma City. For each monthly period, the mean and standard deviation of daily minimum and maximum temperatures were calculated. Based on the mean temperature, the months of June, July and August were found to be the hottest months in a year while December, January and February were considered to be coldest ones. These criteria were used to establish the low temperature and high temperature exposures. Thereafter, precipitation trends were investigated to determine parameters of the wet-dry exposure.

3.1.1 Cyclic Freezing and Thawing Regimen

The cyclic freezing and thawing test was not conducted in accordance with ASTM 666 procedure. Instead, realistic field climatic conditions were found to investigate the effects of low temperature cycling in Oklahoma City. For a given monthly period, the mean and standard deviation of daily-low temperatures were calculated. Then, assuming the temperature profiles follow a standard distribution, the minus one standard deviation (-1s) value was calculated for that monthly period. These values (-1s) were calculated for the coldest months of the year (December, January and February) for years 2004 to 2014. Finally, the average of the latter values was found (20.5°F) and selected as the test temperature for the freeze/thaw regimen. This means that (on average) for 25 days of the month; the daily-low temperature will be greater than 20.5°F during December, January and February. The exposure regimen was replicated in an environmental chamber (Figure 3-1) where the temperature cycled between 20 °F and 40 °F (above freezing point) over a 24-hour period (reminiscent of night and day conditions).

Prior to testing, samples were conditioned at 50% relative humidity for a week and then tightly wrapped in plastic sheet to prevent further moisture loss or gain for that matter during the 3-month exposure time. Once samples conditioned, the environmental chamber was prepared and temperature measurements were taken prior to cycling

samples. The samples were placed in the chamber and subjected to a 4 step 24-hour temperature cycle. Starting at 40°F, the temperature was held for a period of 6 hours. Then, it ramped down for 6 hours until 20°F was reached and held constant for another 6 hours. Afterwards, it ramped up for 6 hours until 40°F was reached. The 24-hour step-cycle simulates temperature fluctuations throughout a day.

Figure 3-1: Environmental chamber and samples placed in environmental chamber for freeze-thaw exposure regimen

3.1.2 Cyclic High Temperature Regimen

There are no standard methods to evaluate the effects of high temperature on concrete material. As such, a similar approach as that used for determining the low temperature exposure was also used for this exposure regimen. For the months of June, July and August, the averages of the daily high and low temperature values were determined. It was found that the average high (2004 to 2014) was 92 °F with a standard deviation of 5.8 °F. As for the average daily low, it was found to be 70 °F with a standard deviation of 4.0 °F. For this time period, the average relative humidity was found to be 42.8%. Therefore, the selected temperature range for cyclic exposure at high temperatures was 64 °F to 98 °F at 43% RH.

Prior to testing, the samples were conditioned for one week in ambient laboratory conditions that was measured to be approximately 40% RH and then placed in the environmental chamber with the set temperature and relative humidity parameters. Here samples were not wrapped in plastic since the chamber could hold humidity settings for the given temperature profile. Once sample conditioned, the environmental chamber was prepared and temperature measurements were taken prior to cycling samples. The samples were placed in the chamber and subjected to a 4-step 24-hour temperature cycle. Starting at 64°F, the temperature was held for a period of 6 hours. Then, it ramped for 6 hours until 98°F was reached and held constant for another 6 hours. Afterwards, it ramped down for 6 hours until 64°F was reached. The 24-hour step-cycle simulates temperature fluctuations throughout a day: morning, afternoon, evening and night.

3.1.3 Cyclic Wetting and Drying Regimen

A similar approach was used to determine the average precipitation and duration of precipitation our infrastructure is exposed to during an annual period. Here, daily precipitations were evaluated and compared with monthly and annual rainfall averages. To determine the rainfall frequency and duration, these values were compared with the Rainfall Frequency Atlas of the US. It was found that for the city of Oklahoma there is approximately 1.1 inches of precipitation in 30 minutes for a recurring period of 1 year. This rainfall was replicated via a fabricated tank and sprinkler system placed in a large walk-in environmental chamber. The exposure temperature and relative humidity was set at 69 °F and 40% RH based on average daily temperatures found for days with recorded precipitation only. These were found to be mainly during the Spring and Fall months.

To replicate the wet-dry activity, the rain apparatus was activated once a day and water was pumped up and delivered onto the samples through spray nozzles for a time period of 30 minutes. During this time, the samples received a water volume in the form of a spray representing approximately 1-inch accumulation. The system was then turned off

and the samples were allowed to dry for the next 23.5 hours. The samples were placed on supports to prevent them from sitting in water. Also, the water was quickly evacuated from sample site into its closed reservoir to prevent local increase in relative humidity. Here, a small room dehumidifier was placed next to the setup within the environmental chamber to aid in lowering the humidity point faster simulating a rainfall and rapid drying period subsequently (Figures 3.2 and 3.3).

Figure 3.2: Rain simulation exposure setup consisting of two interconnected basins with spray nozzle and water reservoir below.

Figure 3.3: Samples placed in rain simulation setup.

3.2 SAMPLE PREPARATION AND CONDITIONING

A conventional concrete mix used for infrastructure construction (e.g. bridge deck) with regional materials was designed according to standard practice. A concrete mixture with 0.45 water/cement ratio with 20% replacement of fly ash and approximate 5% to 8% of air content was selected as the only concrete mixture design in this project. Specimend for this project were prepared in three batches. Each batch consisted of approximately 6 cubic feet of material to cast 20 prisms and 60 cylinders. The descriptions of each material and concrete mix design proportions are shown in Table 3-1.

Table 3-1. Concrete Mixture Design Proportion

Material	Description	Proportion (lb/cy)
Water	Portable water from Stillwater, Oklahoma	279.8
Cement	Type I cement manufactured by Lafarge	502.7
Fly Ash	Class C fly ash from Red Rock	125.7
Coarse Aggregate	5 - 14 mm, Richard Spur	1888
Fine Aggregate	0 - 5 mm, Dover Sand Plant	1228.9
Air Entrainer	Daravair 1000	14.0 oz/cy

Concrete mixing and specimen casting were accomplished according to the procedures in ASTM C192 in a controlled laboratory environment at Bert Cooper Engineering Laboratory at Oklahoma State University. Standard quality control tests of fresh concrete properties, such as slump test (ASTM C143), unit weight test (ASTM C138) and air content test (ASTM C231), were performed on individual concrete batches to ensure consistency in mixture properties.

Standard 4”x8” cylinders according to ASTM C470 and 3” x 4” x 16” prisms which is used in ASTM C666 were casted in a standard manner. After external vibration consolidation, the surface was finished by striking off the extra material with tamping rod or trowel. Finally, plastic cap was placed on each cylinder. Initial curing was performed by covering the specimens with wet burlap loosely sealed with plastic sheet. The samples were demolded after 24 hours of initial curing and were placed in a moist curing room at 73.5°F ± 3.5°F for 28 days (Figure 3.4). The samples were then taken out from the curing room and conditioned for a period of 7 days as described in the previous

sections. The conditioning of the specimens was chosen to represent the true field conditions in which samples are not fully saturated.

Figure 3-4: Specimen moist curing

3.3 SPECIMEN TESTING PROGRAM

The following series of both destructive and nondestructive tests were performed to evaluate the extent in damage for samples exposed to 30-cycle, 60-cycle and 90-cycle of each environmental regimen described previously.

- *ASTM C 39 - Standard Test Method for Compressive Strength of Cylindrical Concrete Specimens*
- *ASTM C 78 - Standard Test Method for Flexural Strength of Concrete (Using Simple Beam with Third-Point Loading)*
- *ASTM C215 - Fundamental Transverse, Longitudinal, and Torsional Resonant Frequencies of Concrete Specimens*

- *ASTM C 597 – Standard Test Method for Pulse velocity through concrete*

These methods were used to assess any overall changes in material stiffness induced by the exposure conditions. To validate nondestructive testing and monitoring results, compression and flexural testing were also conducted to assess the changes in strength characteristics over time. All specimens were tested in a saturated-state to ensure reproducible moisture conditions. To achieve such while minimizing the influence of hydration, the specimens were vacuum-saturated in potable water containing lime and kept immersed under vacuum for 24 hours before testing.

3.3.1 Resonant Frequency Testing

Resonant frequency testing was performed according to the procedure listed in ASTM C215 *Standard Test Method for Fundamental Transverse, Longitudinal, and Torsional Resonant Frequencies of Concrete Specimens*. The method is used to calculate the dynamic Young's modulus of elasticity, the dynamic modulus of rigidity and dynamic Poisson's ratio based on the measurements of different modes (transverse mode, longitudinal mode and torsion mode) of fundamental resonant frequencies of specimen. The test was performed using the Resonance Test Gauge (RTG-1) from Olson Instruments, Inc (Figure 3-5). The test apparatus includes a small hammer acting as an impactor to produce wave excitation, an accelerometer to measure the mechanical vibration under the impactor, connecting cables, and the software that can graphically display the response signal in both time domain and frequency domain.

The three different modes of fundamental frequency were obtained by manipulating different accelerometer attachment locations and different hammer strike points. A small ball-peen hammer that can produce specific frequency range of concrete was used to strike the concrete specimen. At the same time, the acceleration response was recorded by the accelerometer that was attached on the surface and coupled with grease base adhesive agent. Then frequency response could be obtained by converting the time domain response through Fast Fourier Transform. The peak frequency value in frequency spectrum is the resonant frequency. Calculation of dynamic Young's modulus

of Elasticity are based on the following equation 3-1 for cylindrical and prism specimens from the measurement of the samples' fundamental transverse frequency, mass and dimensions [17].

$$E = CMn^2 \qquad \text{Eq. 3-1}$$

where

M : mass of specimen,

n : fundamental transverse frequency,

C : factors calculate from $1.6067(L^3T/d^4)$ for cylindrical specimen and from $0.9464(L^3T/bt^3)$ for prism specimen,

L, b and t : length, width and height of specimen (width and height are only for prism specimen),

d : diameter of cylindrical specimen,

T : correction factor.

Figure 3-5: Experimental setup for resonant frequency test in transverse mode: cylindrical specimen and prism specimen

3.3.2 Ultrasonic Pulse Velocity Testing

Ultrasonic Pulse Velocity (UPV) testing was carried out according to ASTM C597. The instrumentation used in this test was Pundit Lab Ultrasonic Instrument from Proceq, which consists of two 54 kHz transducers, measuring circuit, time display unit and

connecting cable (Figure 3-6). In this method, one transducer held at the one side of the sample produces a longitudinal stress-wave that propagates through the tested sample and is received by the other transducer at a known distance. The pulse velocity can be determined by the ratio of the distance between two transducers and the transit time that is measured by the circuit integral in the equipment.

During the test, water-based coupling agent was applied onto the surfaces of both transducers to ensure a sufficient contact between transducer and concrete. Then, each transducer was firmly pressed against the ends of the concrete cylinder until the display unit provided a stable reading. Both transducers should be approximately in the middle of cylinder, which means they are opposite with each other and a constant distance between them will be obtained. Finally, the whole process was repeated to get second reading by swapping the emitting and receiving transducers. The recorded time readings were considered to be acceptable if the percentage difference of them is less than 2%. The ultrasonic pulse velocity result was calculated as follow [18]:

$$v = L / T \qquad \text{Eq. 3-2}$$

where L stands for the central distance between two transducers and T is the transit time.

Figure 3-6: Experimental setup for ultrasonic pulse velocity test

3.3.3 Compression and Flexural Testing

Compressive strength of cylinder (ASTM C 39) and flexural strength of prism (ASTM C 78) were first conducted on two specimens for each exposure regimen to determine their corresponding ultimate strength. [19-20] Both cylindrical and prism specimens were tested on Instron 5900 series based on the procedures of compressive strength and third-point bending tests described in ASTM C39 and ASTM C78, respectively (Figure 3-7).

Next, cyclic incremental loading tests were performed on both cylindrical and prism specimens for each exposure regimen. The intermediate load levels were setup to be 20%, 40%, 60%, 80% and 100% of their individual ultimate strength determined by the previous standard monotonic load tests. Each load cycle consists of a loading phase, a hold phase and an unloading phase. The reported mechanical properties represent the average of the three samples tested under monotonic and cyclic loading.

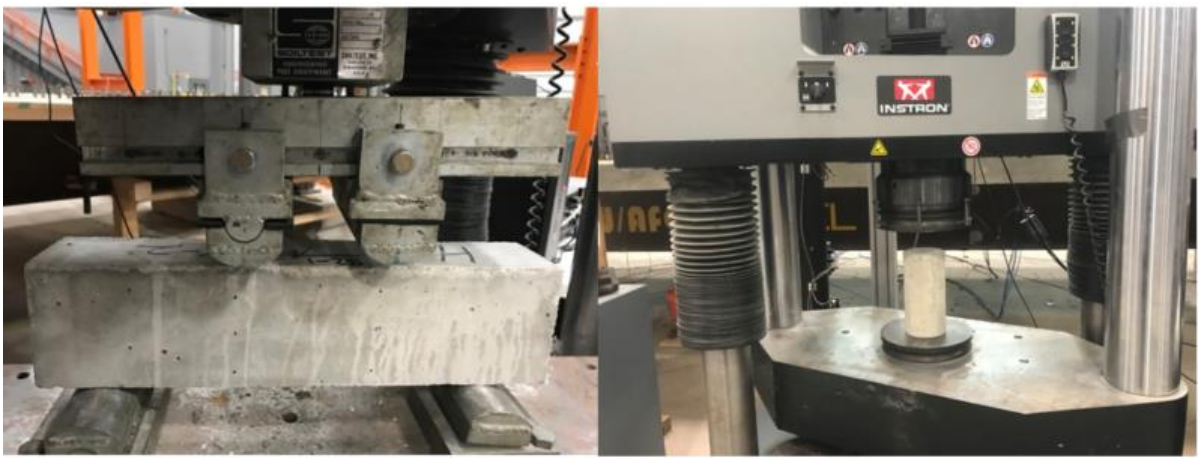

Figure 3-7: Experimental setup of third-point flexural strength test and compressive strength test on universal testing frame.

3.3.4 Acoustic Emission Monitoring

Acoustic emission monitoring was also performed during monotonic and cyclic load testing, which aimed at providing correlations of acoustic emission behavior with the

damage degree of individual sample under different duration of simulated climatic conditions.

A multichannel acoustic emission system Mirco-II Express manufactured by Physical Acoustics Corporation (PAC) was used to perform acoustic emission monitoring. A total of 10 PAC Micro30S sensors with frequency response range of 150–400 kHz were mounted on the surface of the test samples with hot glue. As is shown in Figure 3-8, the arrangement of sensors on cylindrical specimen and prism specimen was designed to be cover the possible failure area of the specimens. Meanwhile, PAC 2/4/6 switch selectable gain single ended and differential preamplifier was used to amplify AE signal before they were sent to AE measurement circuit.

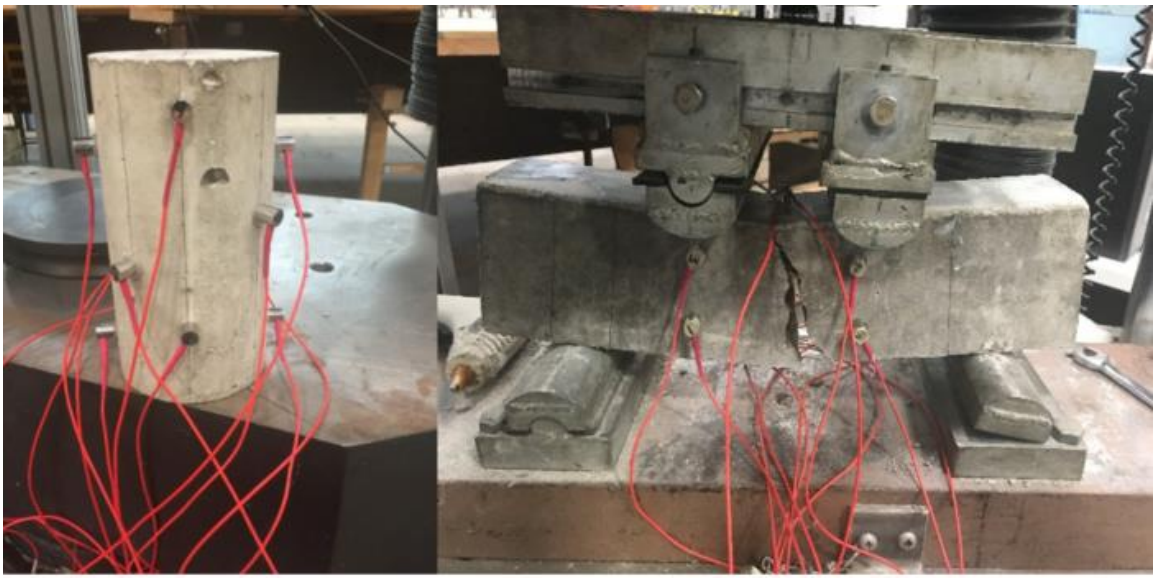

Figure 3-8: AE sensor locations used to monitor cylindrical specimen and prism specimens

The system is controlled by AEwin real-time data acquisition software, which is a window-based program with ability of recording, storing and displaying AE parameters as well as waveform data. It allows the users to customize the data collection settings related to both hardware and software to fit their specific need. These software settings were chosen based on the common practices of acoustic emission testing in concrete material. For example, the 50dB threshold and the band pass filter with a cutoff frequency range from 100kHz to 400kHz were determined to eliminate the background

noises from load testing equipment and general laboratory environment. Three AE hit determination parameters, hit definition time (HDT), hit lockout time (HLT) and peak definition time (PDT), were set to be 400 μs , 200 μs and 200, respectively. In addition, nearly all the AE hit driven parameters, such as amplitude, duration, energy and etc., were activated for collection of data. Other settings of the software were left to be default numbers as recommendations in the AEwin software manual. Before recording AE monitoring data, auto sensor test (AST) and pencil lead breaking test (PLBT) were performed to verify if the sensors were properly attached and working as per ASTM E2374 [21]. The raw AE data from the tests were converted into ASCII files and then to be used to analyze and visualize by MATLAB.

4. RESULTS AND DISCUSSION

As concrete materials are subjected to various external events causing it to develop internal tensile stresses and strains, the mechanical effects will lead to physical deterioration over time that will alter its engineering properties. In the field, timely identification of such processes as they initiate and progress is of importance. Through analysis of the obtained experimental results, the next chapter presents a discussion on the behavior by which the concrete specimens responded to their exposure regimes.

4.1 MECHANICAL TESTING

First, to determine the effects of each exposure regimen on the materials mechanical properties, compressive strength testing was conducted on the cylindrical samples and flexural testing was conducted on the beam samples. Here, a loss in mechanical properties could indicate a change in the material's physical integrity caused by the development of microcracking. Test results are presented in the following subsections along with a statistical analysis of equality of the means.

4.1.1 Compressive Strength Testing

Table 4-1 presents the average compressive strength results along with the standard deviations and coefficients of variation (COV) obtained for the three exposure regimens (H-T, F-T and W-D) and for their respective exposure cycles: 0, 30, 60 and 90 cycles. Values representing 0 cycles serve has the control for which properties were measured after sample conditioning period, thus time 0 of exposure period. For each regimen and number of exposure cycles, the results of a comparative analysis (percent change and difference between the samples' means) are also given. The returned p-value of a t-test conducted between two sets are presented in Table 3-1 to determine whether the

percent change in test results are significant or not. Here a confidence level of 95.0% is used for that purpose ($\alpha = 0.050$).

Looking at the coefficients of variation calculated for each exposure regimen, they varied between 5.7% and 16.5% except for one specimen, 30 cycles of W-D, which recorded a variation of 1.2%. Although coefficients of variation are above that prescribed in ASTM C39, this trend is often seen for degraded samples subjected to mechanical testing. The differences in the extent of damage between the three sample replicates will result in this higher coefficient of variation. [22] Due to this fact, it may be difficult to evaluate the differences between the sample means of two data sets of different variance. This seen for samples exposed to high temperature (H-T) cycling and wet dry cycling. There are no clear trends after 30 and 60 exposure cycles. However, there is a significant drop in strength for the cyclic freeze-thaw exposure for specimens exposed to 30 and 60 cycles. After 90 exposure cycles, the results of the t-test indicate that a 25.2%, 24.3% and 28.8% drop in compressive strength for the H-T, F-T and W-D regimens respectively is significant in comparison to their respective control specimen.

Table 4-1: Compressive strength results and sample statistics for high temperature variance, cyclic freeze-thaw and cyclic wet-dry exposure regimens.

Specimen	Average Strength (psi)	Standard Deviation (psi)	Coefficient Of Variation (%)	Percent Change (%) with respect to control	F-Test (p-value) with respect to control	t-Test (p-value) with respect to control
H-T-0	5550	139	2.5	-	-	-
H-T-30	5007	826	16.5	-9.8	0.055	0.324
H-T-60	5656	475	8.4	1.9	0.151	0.723
H-T-90	4155	532	12.8	-25.2	0.123	0.019
W-D-0	5226	80	1.5	-	-	-
W-D -30	4147	482	11.6	-20.7	0.054	0.035
W-D -60	3927	349	8.9	-24.9	0.101	0.007
W-D -90	3957	224	5.7	-24.3	0.259	0.001
F-T-0	4903	94	1.9	-	-	-
F-T-30	4513	53	1.2	-8.0	0.844	0.026
F-T-60	5275	388	7.4	7.6	0.082	0.305
F-T-90	3493	199	5.7	-28.8	0.268	0.004

4.1.2 Flexural Strength Testing

Table 4-2 presents the test results and sample statistics obtained for the flexural test conducted on the prismatic specimen. Here, due to experimental manipulation error, there are no results obtained for the freezing and thawing regimen. The level in flexural strength lost is not has great has that reported for the compressive strength study. Flexural strength loss varies between 3.2% and 14.9% for all exposure regimens over their exposure period. Again, there are no discernable trends for the high temperature. As for the wet-dry exposure, there is a gradual loss in properties between 0 and 90 cycles but, insignificant according to the returned p-values.

Table 4-2: Flexural strength results and sample statistics for high temperature variance and cyclic wet-dry exposure regimens.

Specimen	Average Strength (psi)	Standard Deviation (psi)	Coefficient Of Variation (%)	Percent Change (%) with respect to control	F-Test (p-value) with respect to control	t-Test (p-value) with respect to control
H-T-0	696	14	2.1	-	-	-
H-T-30	592	51	8.7	-14.9	0.148	0.028
H-T-60	700	20	2.9	0.6	0.683	0.790
H-T-90	666	104	15.6	-4.3	0.038	0.753
W-D-0	677	13	2.0	-	-	-
W-D -30	655	42	6.4	-3.2	0.180	0.528
W-D -60	629	28	4.5	-7.1	0.268	0.140
W-D -90	584	59	10.1	-13.8	0.097	0.093

4.2 NONDESTRUCTIVE TESTING

Prior to destructive mechanical testing, a series of nondestructive tests were performed. Ultrasonic and resonant frequency testing were performed to assess the change in physical properties of the samples. These methods have proven to be more sensitive to microstructural disparities than mechanical testing. [22-23] The velocity of a transient wave is dependent on the elastic modulus and density of the material; its value will not change if the distance traveled changes. This is inferred by the basic wave velocity equation relating frequency to wavelength. When studying wave propagation through a

heterogeneous material such as concrete, a transient wave will encounter boundaries (changes in medium densities) which will influence its behavior because of the change in acoustical impedance at the boundary (i.e. boundary behavior). First, a portion of an incident wave traveling through a solid medium will be reflected once it encounters another solid medium boundary of different density. The reflected wave will travel back into the medium at the same velocity. The other portion of the transient wave will continue traveling through the second medium at a different velocity. The degree of reflection depends on the difference in acoustical impedances. As a concrete sample degrades due to the generation of microcracks, each crack will create an additional boundary with a change in medium properties. In this case, the void would be filled with water since the samples were vacuum saturated prior to testing. The speed of a stress-wave is lower for water than for concrete. Therefore, the presence of water-filled cracks will contribute to lowering the recorded wave speed during an ultrasonic pulse velocity test. In the case of the resonant frequency test, the lowered wave speed will also contribute to lowering the recorded frequency since the wavelength (or sample geometry) does not change. [24]

4.2.1 Resonant Frequency Testing

The results of the resonant frequency test conducted on cylindrical and prismatic specimens respectively are presented in Tables 4-3 and 4-4. Looking at the obtained coefficients of variation, they varied between 0.1% and 5.0% for both sample types, which is lower than that observed for destructive testing. This permitted an analysis of differences between the means even if the percent change is not as prominent as that observed for destructive testing.

As previously mentioned, the effects on the concrete material caused by all three regimen types contributed to lowering the resonant frequency thus the calculated dynamic modulus of elasticity. After 30 cycles of exposure, the cylindrical specimen type demonstrated a significant reduction in dynamic modulus of elasticity with an 11.0%, 5.3% and 9.9% drop for the high-temperature, freeze-thaw and wet-dry exposure types

respectively. Similarly, the prism specimens recorded a drop of 9.6% and 11.2% for high-temperature and wet-dry exposure types respectively. With an increase number of cycles, there is a noticeable progression in damage for both sample type as the measured dynamic modulus of elasticity continues to drop. However, the rate in damage progression is not as significant has that seen for the first 30 cycles of exposure.

Table 4-3: Dynamic Modulus of Elasticity results and sample statistics for cylindrical specimens, high temperature variance, cyclic freeze-thaw and cyclic wet-dry exposure regimens.

Specimen	Average Strength (psi)	Standard Deviation (psi)	Coefficient Of Variation (%)	Percent Change (%) with respect to control	F-Test (p-value) with respect to control	t-Test (p-value) with respect to control
H-T-0	5480	65	1.2	-	-	-
H-T-30	4877	242	5.0	-11.0	-11.0	0.014
H-T-60	4739	217	4.4	-10.7	-10.7	0.011
H-T-90	4630	53	1.0	-15.2	-15.2	0.001
W-D-0	5321	25	0.5	-	-	-
W-D -30	5038	110	2.2	-5.3	-5.3	0.023
W-D -60	4893	96	2.0	-8.1	-8.1	0.004
W-D -90	4801	236	4.9	-9.8	-9.8	0.088
F-T-0	5161	27	0.5	-	-	-
F-T-30	4652	102	2.2	-9.9	-9.9	0.002
F-T-60	4629	172	3.7	-10.3	-10.3	0.045
F-T-90	4515	74	1.7	-12.5	-12.5	3.2 E-4

Table 4-4: Dynamic Modulus of Elasticity results and sample statistics for prism specimens, high temperature variance and cyclic wet-dry exposure regimens.

Specimen	Average Strength (psi)	Standard Deviation (psi)	Coefficient Of Variation (%)	Percent Change (%) with respect to control	F-Test (p-value) with respect to control	t-Test (p-value) with respect to control
H-T-0	5374	122	2.3	-	-	-
H-T-30	4857	138	2.8	-9.6	0.879	0.008
H-T-60	4840	165	3.6	-10.1	0.666	0.011
H-T-90	4724	63	1.3	-12.1	0.422	0.001
W-D-0	5356	62	1.2	-	-	-
W-D -30	4757	126	2.6	-11.2	0.628	0.004
W-D -60	4740	6	0.1	-11.5	0.019	0.005
W-D -90	4427	69	1.6	-17.4	0.883	1.4 E -4

4.2.2 Ultrasonic Pulse Velocity Testing

Ultrasonic pulse velocity testing was conducted on the cylinder samples prior to destructive testing. As seen in Table 4-5, the coefficients of variation varied between 0.3% and 2.9%, which is within an acceptable range for potentially damaged concrete. [23] Again, the results follow that previously reported for other destructive and nondestructive methods. There is a reduction in wave speed with an increased number of cycle exposure, which would indicate the presence of damage to the concrete matrix. However, the only exposure regimen demonstrating significant change in measurement is the cyclic freeze-thaw exposure type: 6.7%, 6.9% and 6.6% after 30, 60 and 90 cycles of exposure. It would seem that damage initiated in the first 30 cycles, and no significant damage occurred thereafter. As for the other two exposure regimens, the rate in percent change from the control is gradually decreasing.

Table 4-5: Ultrasonic Pulse Velocity results and sample statistics for high temperature variance, cyclic freeze-thaw and cyclic wet-dry exposure regimens.

Specimen	Average Strength (psi)	Standard Deviation (psi)	Coefficient Of Variation (%)	Percent Change (%) with respect to control	F-Test (p-value) with respect to control	t-Test (p-value) with respect to control
H-T-0	16,667	123	0.7	-	-	-
H-T-30	16,475	63	0.4	-1.2	0.418	0.074
H-T-60	16,193	70	0.4	-2.8	0.491	0.081
H-T-90	16,148	186	1.2	-3.1	0.611	0.058
W-D-0	16,574	76	0.5	-	-	-
W-D -30	15,460	341	2.2	-6.7	0.094	0.011
W-D -60	15,427	204	1.3	-6.9	0.243	0.009
W-D -90	15,473	405	2.6	-6.6	0.076	0.011
F-T-0	16,482	54	0.3	-	-	-
F-T-30	16,023	180	1.1	-2.8	0.990	0.059
F-T-60	15,632	448	2.9	-5.1	0.029	0.056
F-T-90	15,636	362	2.3	-5.1	0.044	0.078

4.3 ACOUSTIC EMISSION MONITORING

The results of the destructive and nondestructive test programs provide insight on whether there may be significant damage present in the concrete samples that may be

attributed to the effects of the exposure regimens. To confirm loss in engineering properties, acoustic emission monitoring was performed during destructive testing which may provide additional information to support that found for this destructive and nondestructive study as well as providing an indication on the extent of damage caused by the exposure regimens. Two different loading schemes were performed for both cylinder and prism samples. The first, monotonic loading up to failure and, the second, cyclic incremental step-load where samples were loaded and unloaded in increments of 20% of ultimate strength up to sample failure. During loading, the level of emissivity may provide an indication of material integrity. For this study, a parameter-based analysis is performed. The intensity of hits and related amplitude along with cumulative energy are presented in the following sub-sections for each regimen type.

4.3.1 High Temperature Variance

4.3.1.1 Monotonic Load Test - Cylindrical Specimen

As previously discussed, the results of the compression test indicated a significant drop in strength for the specimen subjected to 90 cycles. Seen in Figures 4-1 and 4-2, the trend in emissivity and related cumulative energy for specimens subjected to 30 and 60 cycles are different from that observed for the 90-cycle exposure, which supports previous findings.

Generally observed for concrete materials, increased AE activity at low compressive load level, 0 to approximately 30% of ultimate stress, may correspond to internal movement or compaction of aggregate and cementitious phases under the effects of compression (Figure 4-1) causing friction-based AE activity. This is also marked by a higher rate in cumulative energy gain at the beginning of the test (Figure 4-2).

As the stress level increases from 30% to 70% of ultimate stress level, there is a decrease in activity for the specimens subjected to 30-cycle (Figure 4-1a) and 60-cycle (Figure 4-1b); whereas, the specimen subject to 90-cycle demonstrated an increasing

trend of AE activity (Figure 4-1c). For the latter, the cumulative energy plots also support findings by demonstrating an increasing rate in cumulative energy as opposed to no gain for the other two specimens. Here, the presence of micro-damage within the matrix may have prompted crack growth during loading that ultimately lead to a 25.2% decrease in strength.

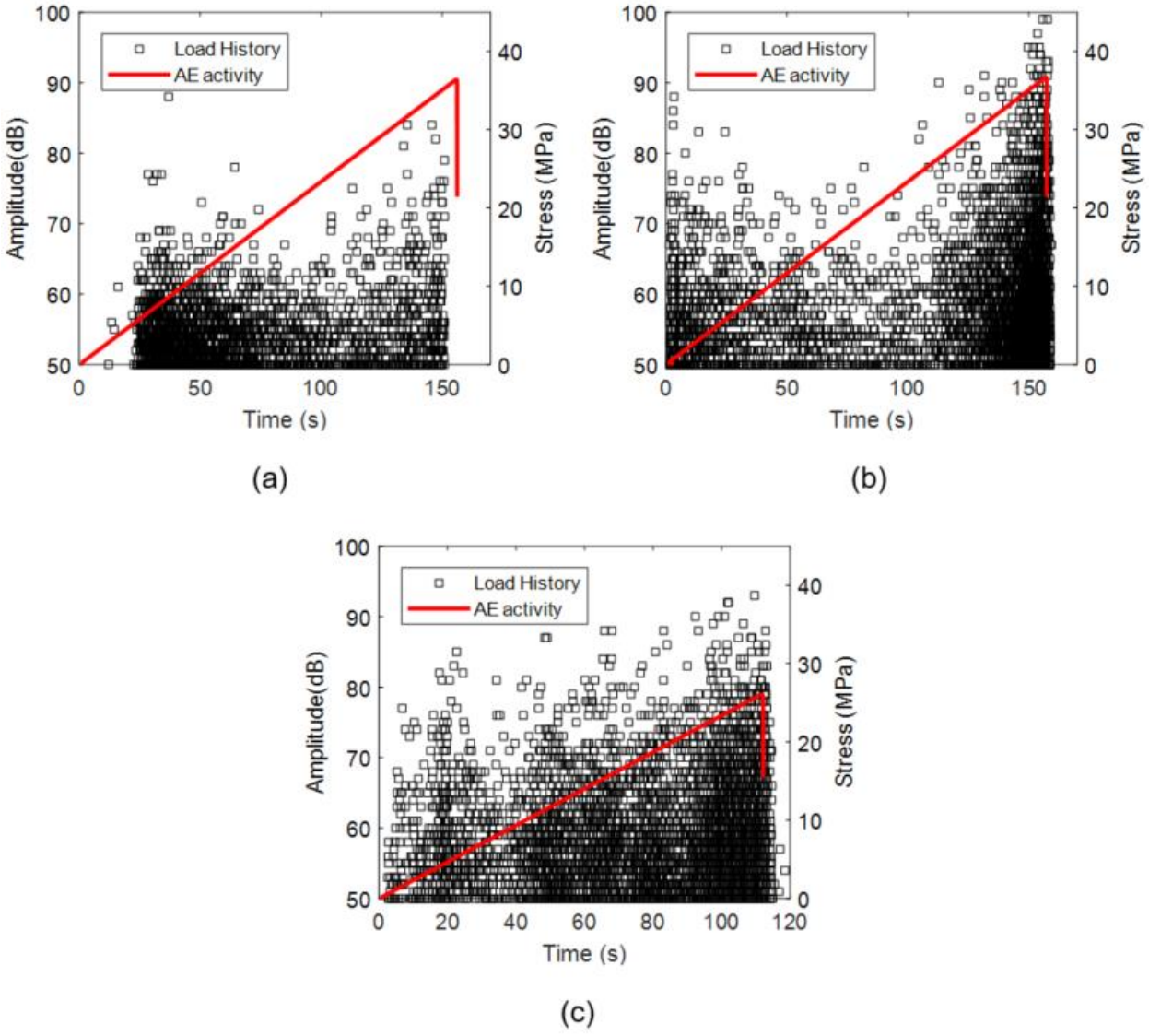

Figure 4-1: Acoustic emission activity and stress history with time for cylindrical specimens under H-T exposure regimen: (a) after 30-cycle; (b) after 60-cycle; (c) after 90-cycle

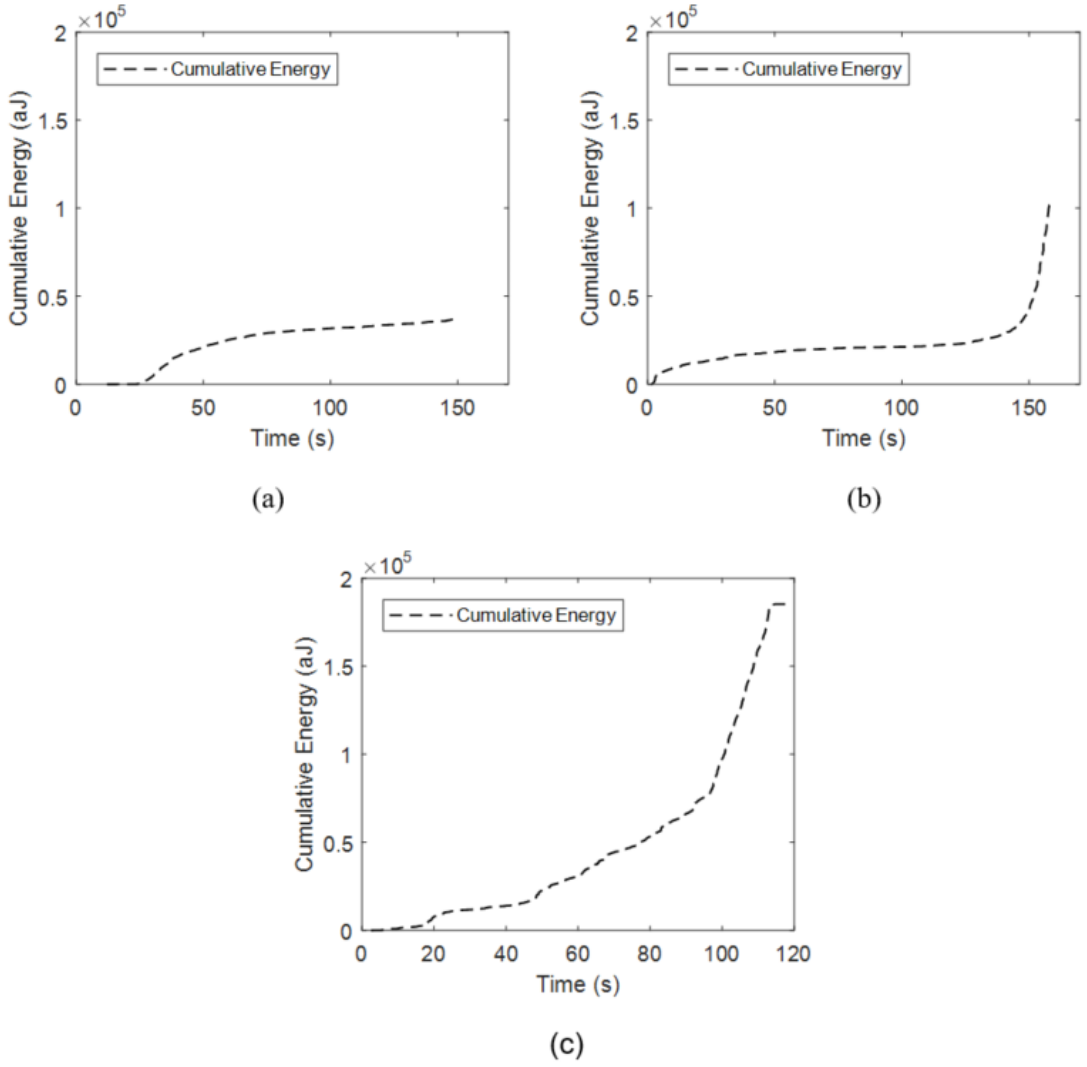

Figure 4-2: Cumulative energy with time for cylindrical specimens under H-T exposure regimen: (a) after 30-cycle; (b) after 60-cycle; (c) after 90-cycle

4.3.1.2 Cyclic Load Test - Cylindrical Specimen

A similar behavior is observed for the cyclic step loading profile. For specimens exposed to 30 and 60 high temperature cycles (Figures 4-3a and 4-3b), there is an initial high degree in emissivity for the first loading-step (up to 20% of compressive strength) followed by very little activity up to the last loading-step where the specimens generated a high level of AE activity as cracking initiated and propagated causing failure.

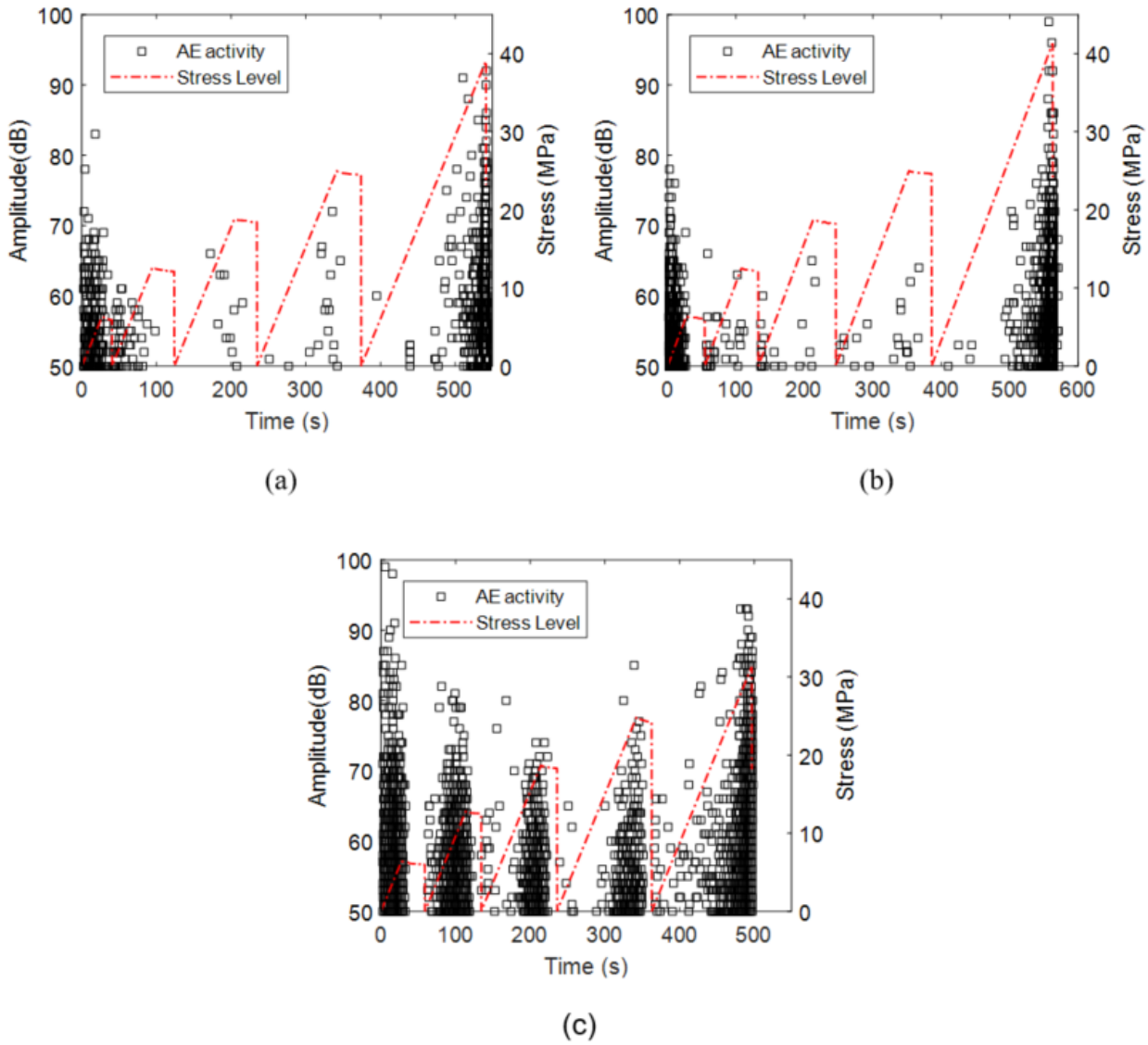

Figure 4-3: Acoustic emission activity and stress history with time for cylindrical specimens under H-T exposure regimen: (a) after 30-cycle; (b) after 60-cycle; (c) after 90-cycle

This behavior is not observed for the specimen exposed to 90 cycles of high temperature variance. There is a marked increase in activity for each load level also demonstrating both Kaiser and Felicity effect with an increase in loading level (figure 4-4c). This behavior is indicative of present damage within the material. With each load level, the microcracks can open and close generating friction type emissions. As step-

loading increases, cracks grow instigating further damage to the material. This is also represented in the increased cumulative energy for this regimen (Figure 4-4c).

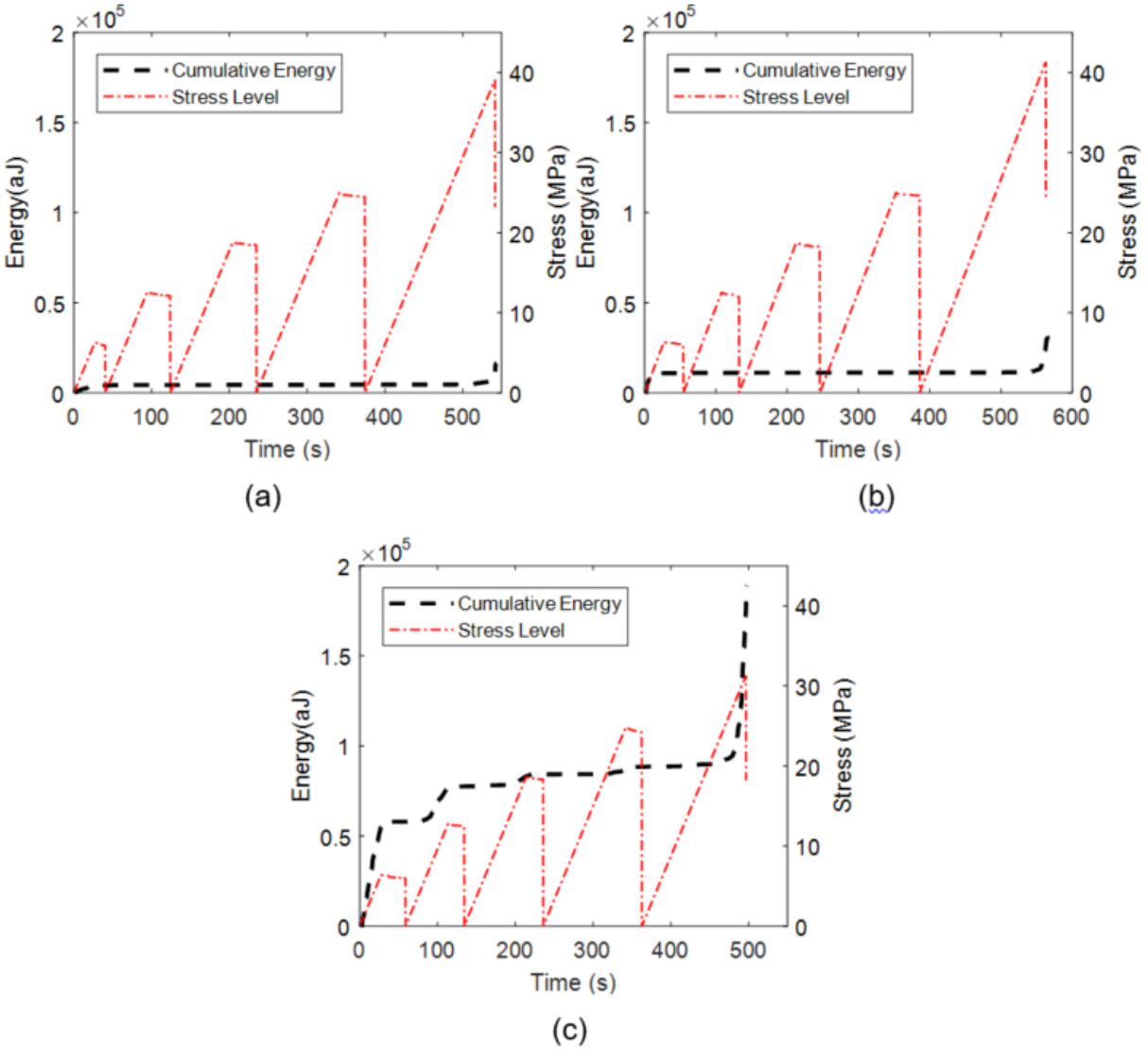

Figure 4-4: Cumulative energy with time for cylindrical specimens under H-T exposure regimen: (a) after 30-cycle; (b) after 60-cycle; (c) after 90-cycle

4.3.1.3 Monotonic Load Test - Prism Specimen

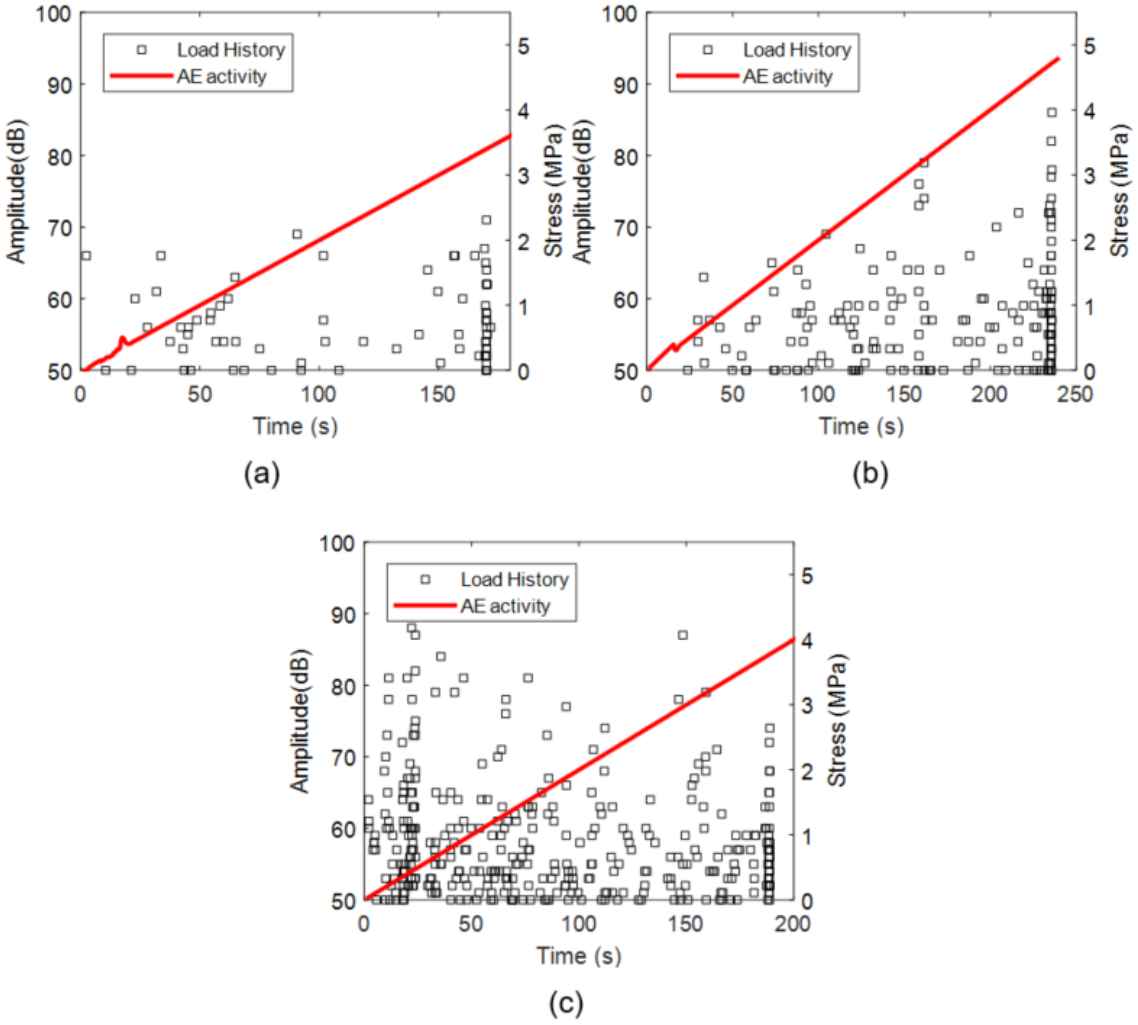

Figure 4-5: Acoustic emission activity and stress history with time for prism specimens under H-T exposure regimen: (a) after 30-cycle; (b) after 60-cycle; (c) after 90-cycle

Figures 4-5 and 4-6 demonstrate the acoustic emission activity during monotonic flexural loading. As seen, the level in emissivity is much lower than that observed for the compression test. This may be attributed to the internal stress distribution and failure mechanism of a prism under flexural load. Here, the initial physical effects due to crushing under compressive loading emitting friction type AE signals are not as

prominent. The development of tensile stress contributes to crack opening and propagation up to failure resulting in a fewer number of hits but of higher energy. With an increased number of exposure cycles, there is an increased number of hits throughout the flexural load test. The presence of microcracks may have altered the failure mechanisms of the prism generating a greater number of nucleation sites and propagation.

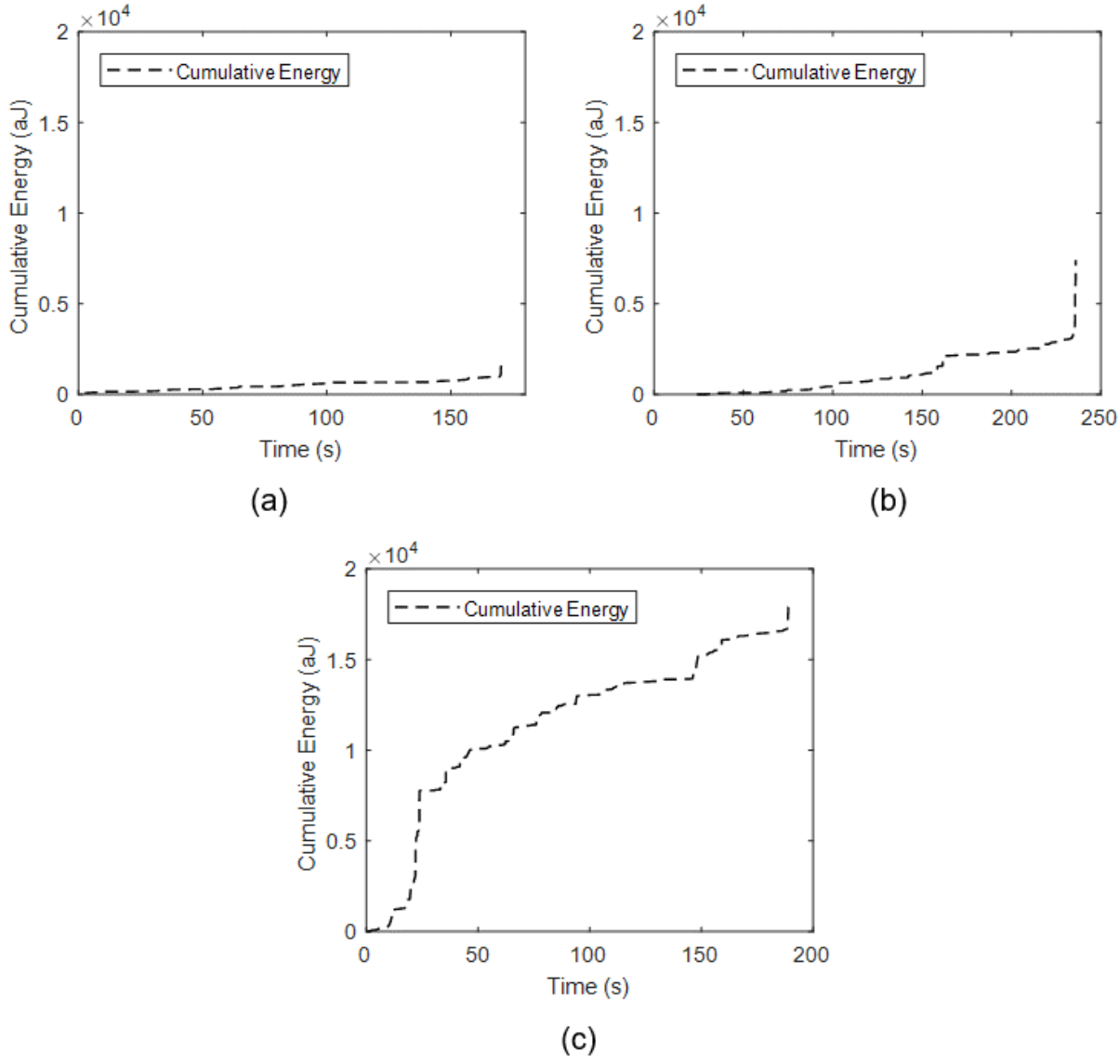

Figure 4-6: Cumulative energy with time for prism specimens under H-T exposure regimen: (a) after 30-cycle; (b) after 60-cycle; (c) after 90-cycle

4.3.1.4 Cyclic Load Test - Prism Specimen

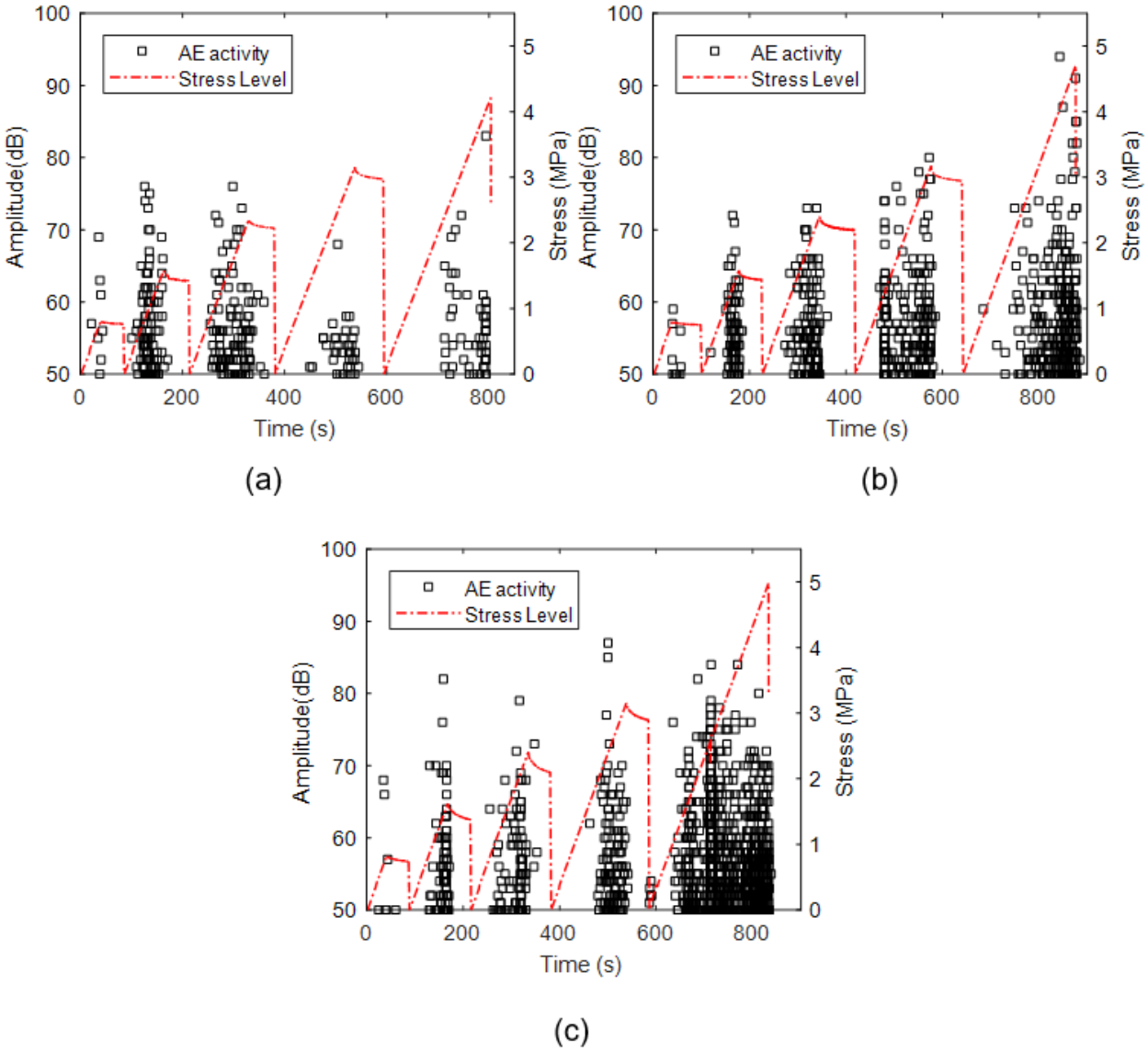

Figure 4-7: Acoustic emission activity and stress history with time for prism specimens under H-T exposure regimen: (a) after 30-cycle; (b) after 60-cycle; (c) after 90-cycle

Demonstrated in Figures 4-7 and 4-8, AE activity during cyclic step-loading for samples exposed to 30 and 60 high-temperature cycles demonstrated mostly a Kaiser effect with each increasing load cycle followed by no activity upon unloading. This is an indication that the material may not have incurred any forms of damage affecting its integrity. For the 90 cycles of H-T exposure, there is presence of the Felicity effect for the last loading

cycle were AE activity started from the beginning of loading up to failure. This is also accompanied by an increase in cumulative energy for this exposure regimen: 10,000 aJ, 20,000 aJ and 35,000 aJ for the 30-cycle, 60-cycle and 90-cycle exposures respectively. This supports previous assumptions that high temperature exposure generated a form of damage after 90 cycles of exposure.

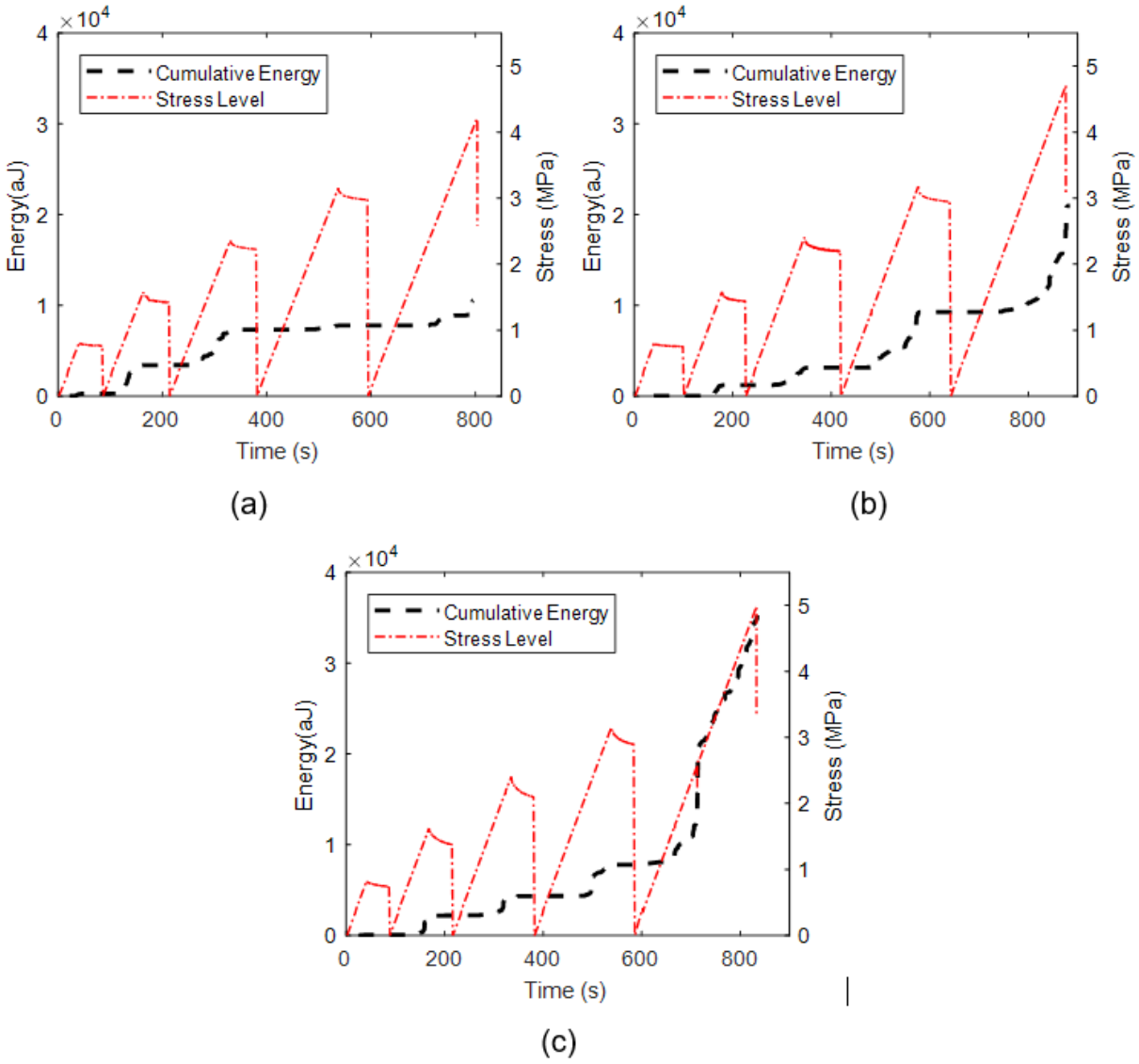

Figure 4-8: Cumulative energy with time for prism specimens under H-T exposure regimen: (a) after 30-cycle; (b) after 60-cycle; (c) after 90-cycle

4.3.2 Cyclic Freeze-thaw

4.3.2.1 Monotonic Load Test - Cylindrical Specimen

Previously discussed in sections 4.1 and 4.2, the extent in damage caused by freeze-thaw exposure was deemed significant after only 30 cycles of exposure to the regimen. Although the trend indicated that the level of damage progressed, it may not have been substantial between 30 and 90 cycles.

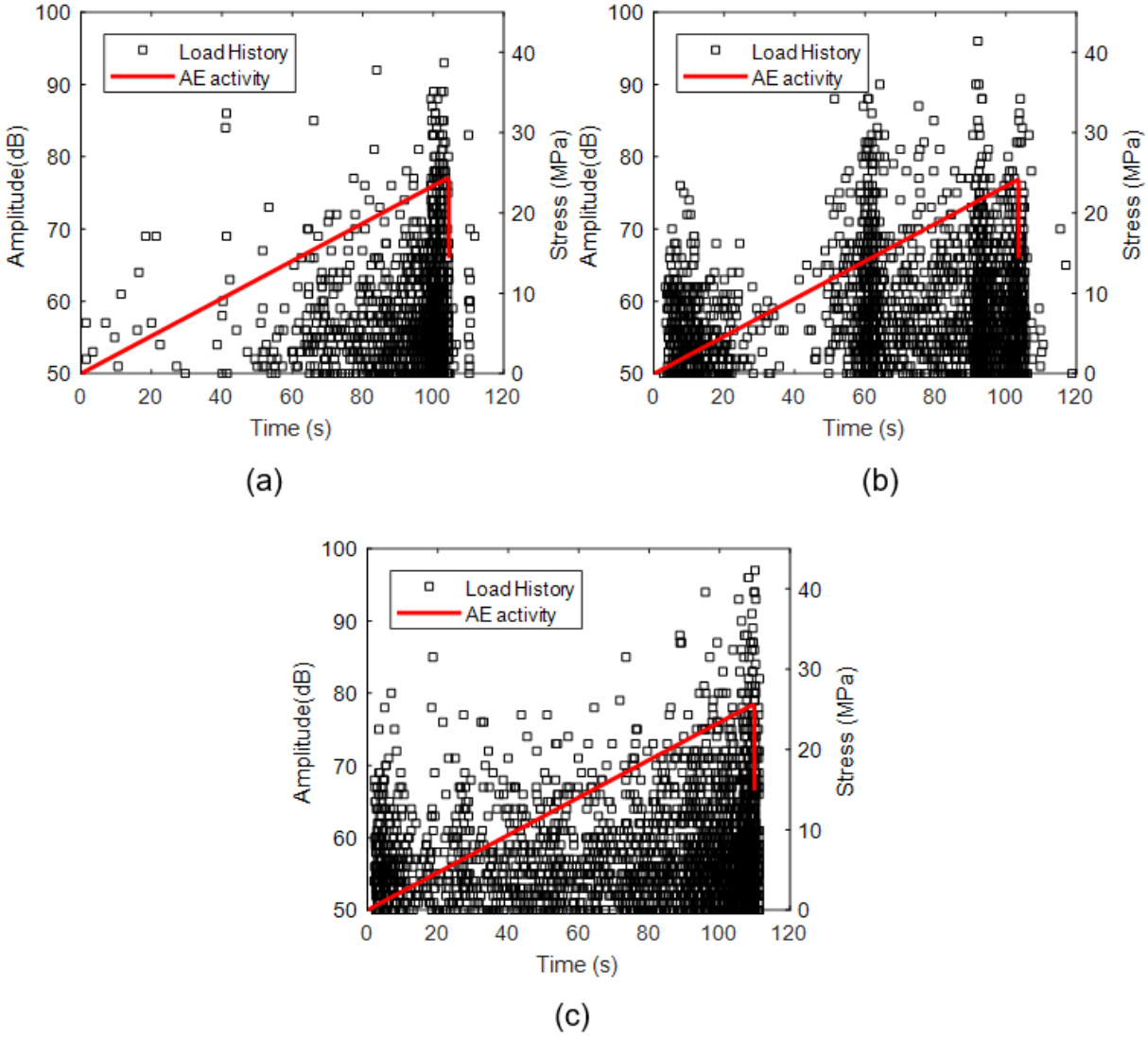

Figure 4-9: Acoustic emission activity and stress history with time for cylindrical specimens under freeze-thaw exposure regimen: (a) after 30-cycle; (b) after 60-cycle; (c) after 90-cycle

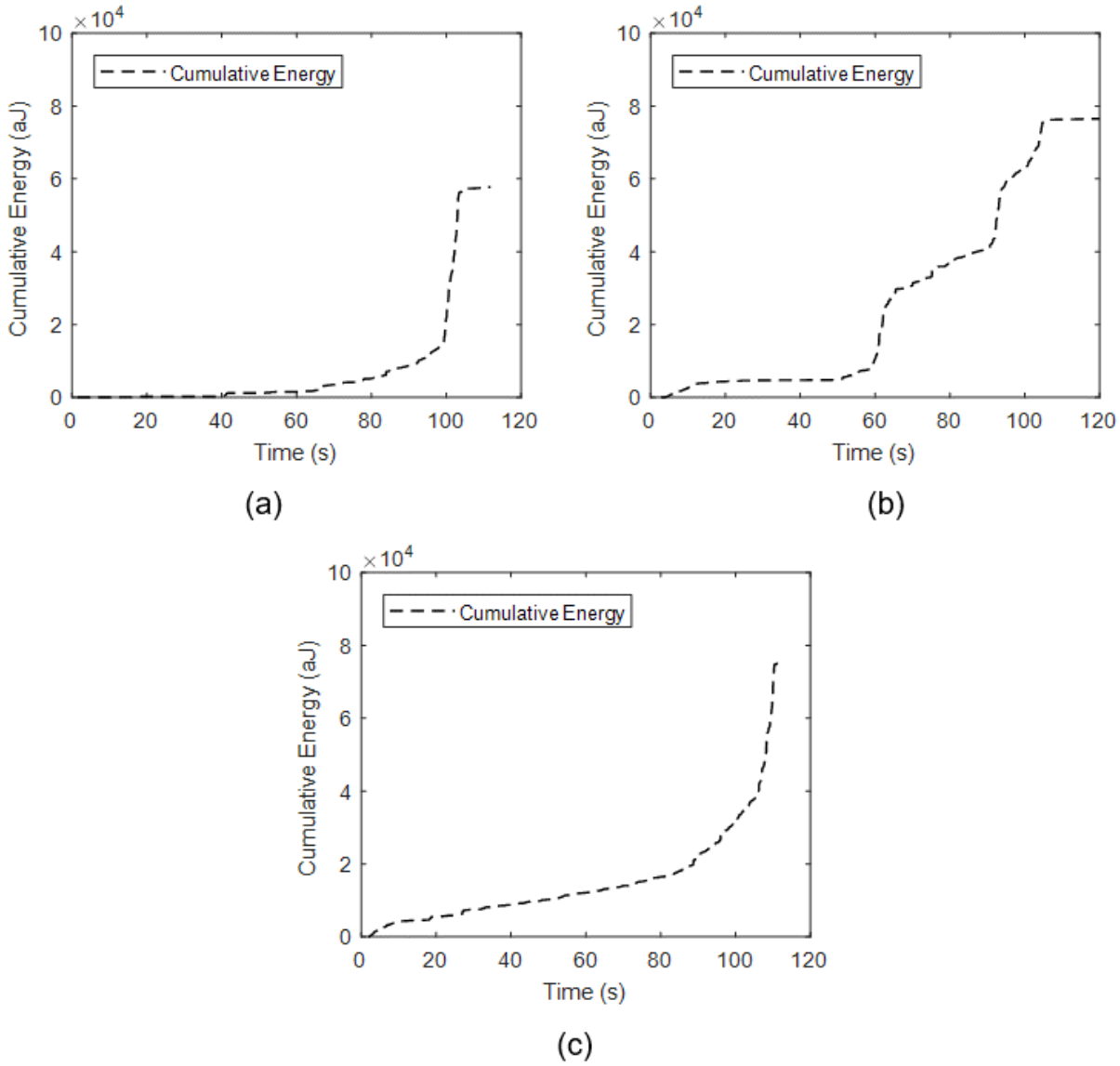

Figure 4-10: Cumulative energy with time for cylindrical specimens under freeze-thaw exposure regimen: (a) after 30-cycle; (b) after 60-cycle; (c) after 90-cycle

Looking at the emissivity figures during loading for each cycles of exposure, there seems to be an increase in the number of hits with an increase in exposure cycles (Figure 4-9). However, the trends observed for the cumulative energy in Figure 4-10 present a similar behavior for all three specimens. The cumulative energy recorded up to failure are approximately 60,000 aJ for the sample subjected to 30 F-T cycles and 80,000 aJ for the samples exposed to 60 and 90 F-T cycles.

4.3.2.2 Cyclic Load Test - Cylindrical Specimen

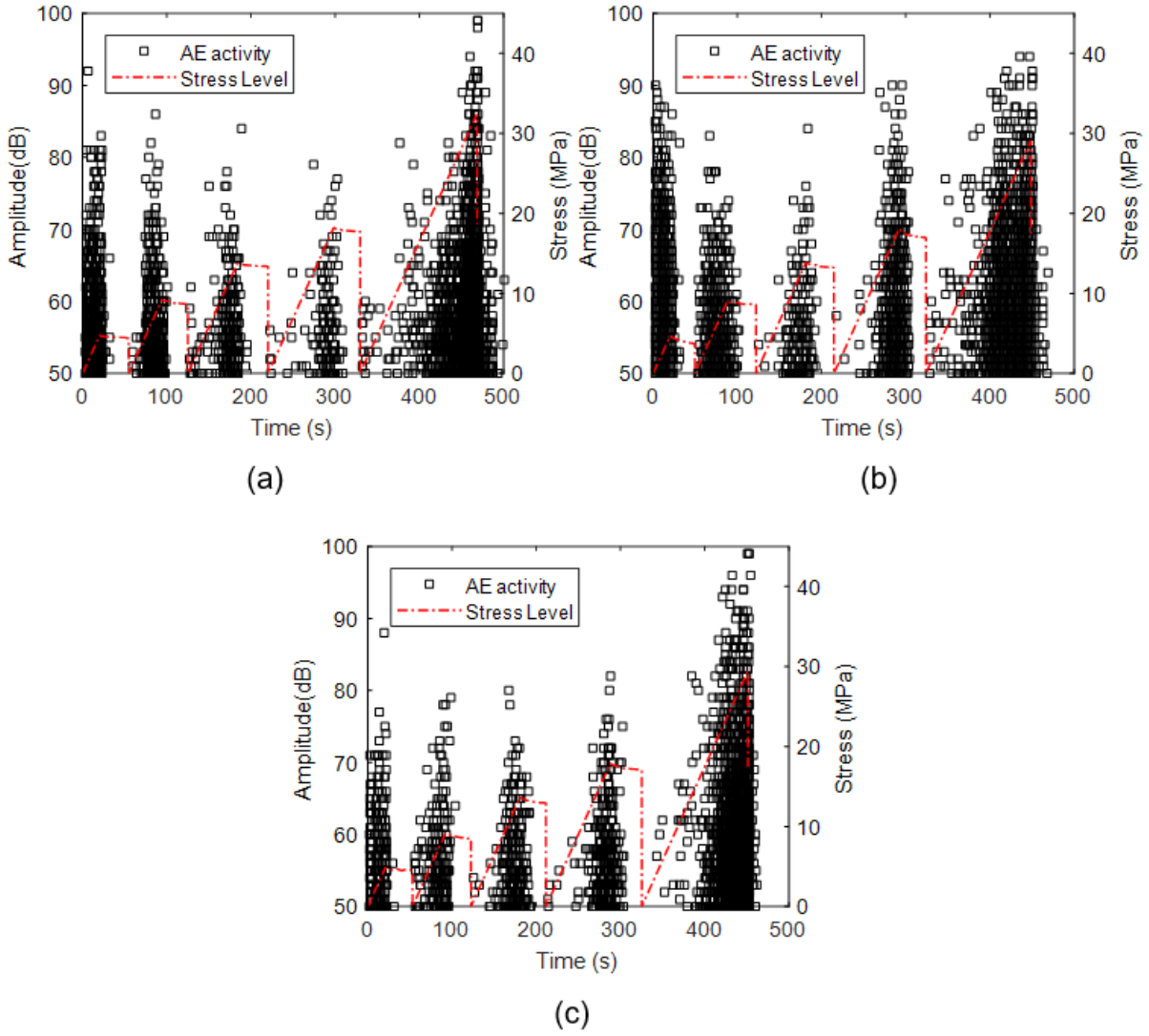

Figure 4-11: Acoustic emission activity and stress history with time for cylindrical specimens under freeze-thaw exposure regimen: (a) after 30-cycle; (b) after 60-cycle; (c) after 90-cycle

The behavior in emissivity during the cyclic load test also confirms the assumption that the samples sustained some form of damage after only 30 cycles of freezing and thawing exposure. Seen in Figure 4.11 for all three exposure cycles, with each increasing load step, there are recorded AE hits prior to achieving the previous load level. This felicity effect may be indicative of micro-disparities opening and closing during loading causing friction-based emissions or crack growth. As that seen for

monotonic loading, the trends in cumulative energy are similar for all three specimens as well (Figure 4-11) corroborating that previously found for monotonic loading.

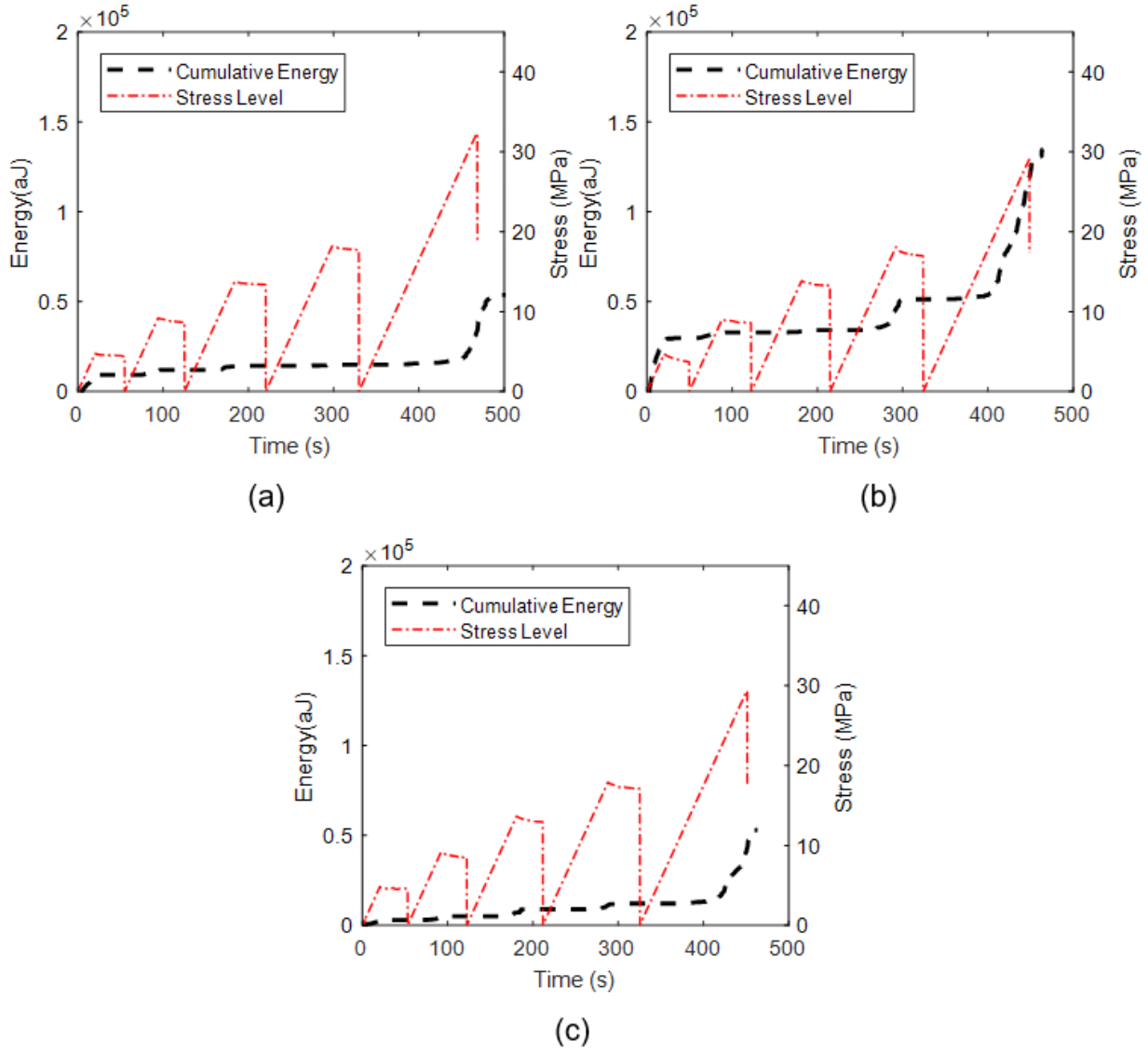

Figure 4-12: Cumulative energy with time for cylindrical specimens under freeze-thaw exposure regimen: (a) after 30-cycle; (b) after 60-cycle; (c) after 90-cycle

4.3.3 Cyclic Wet-dry

4.3.3.1 Monotonic Load Test - Cylindrical Specimen

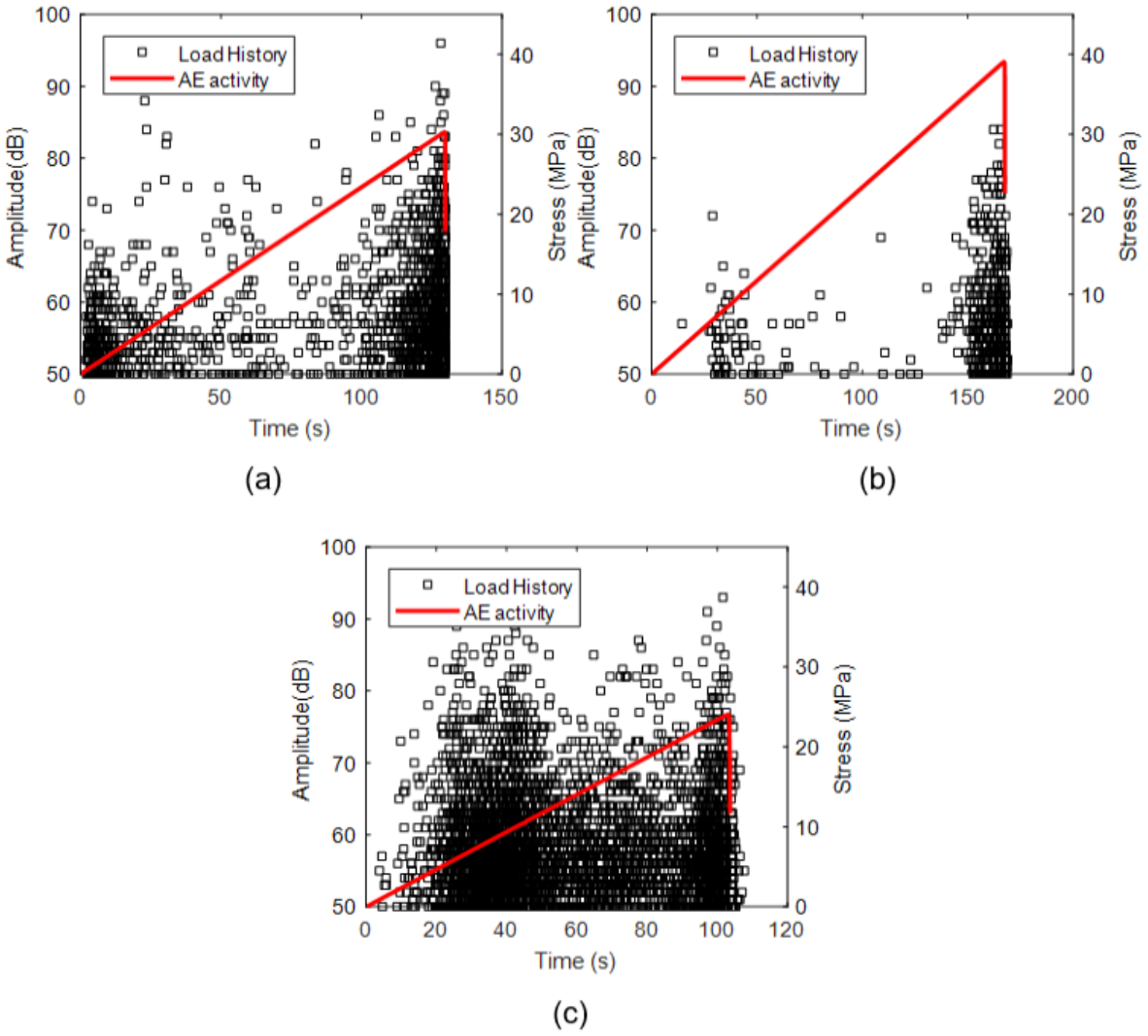

Figure 4-13: Acoustic emission activity and stress history with time for cylindrical specimens under cyclic wet-dry exposure regimen: (a) after 30-cycle; (b) after 60-cycle; (c) after 90-cycle

Again, from Figure 4-13, AE activity is higher at the beginning of loading up to 30% of the ultimate stress and followed by a reduction in activity until the sample approaches failure loads. This is reflected in the cumulative energy graphs where energy remains low up to failure of the samples. As previously discussed for the high temperature exposure regimen, this may be attributed to the fact that the samples did not sustain a significant level of damage due to this exposure type. Only after 90 cycles of wetting and drying is a substantial increase in AE activity observable.

The increase in the number of hits and cumulative energy (Figures 4-13c and 4-14c) may be indicative of damage induced by the exposure regimen. This may have led to the lower compressive strength recorded for the 90-cycle W-D exposure.

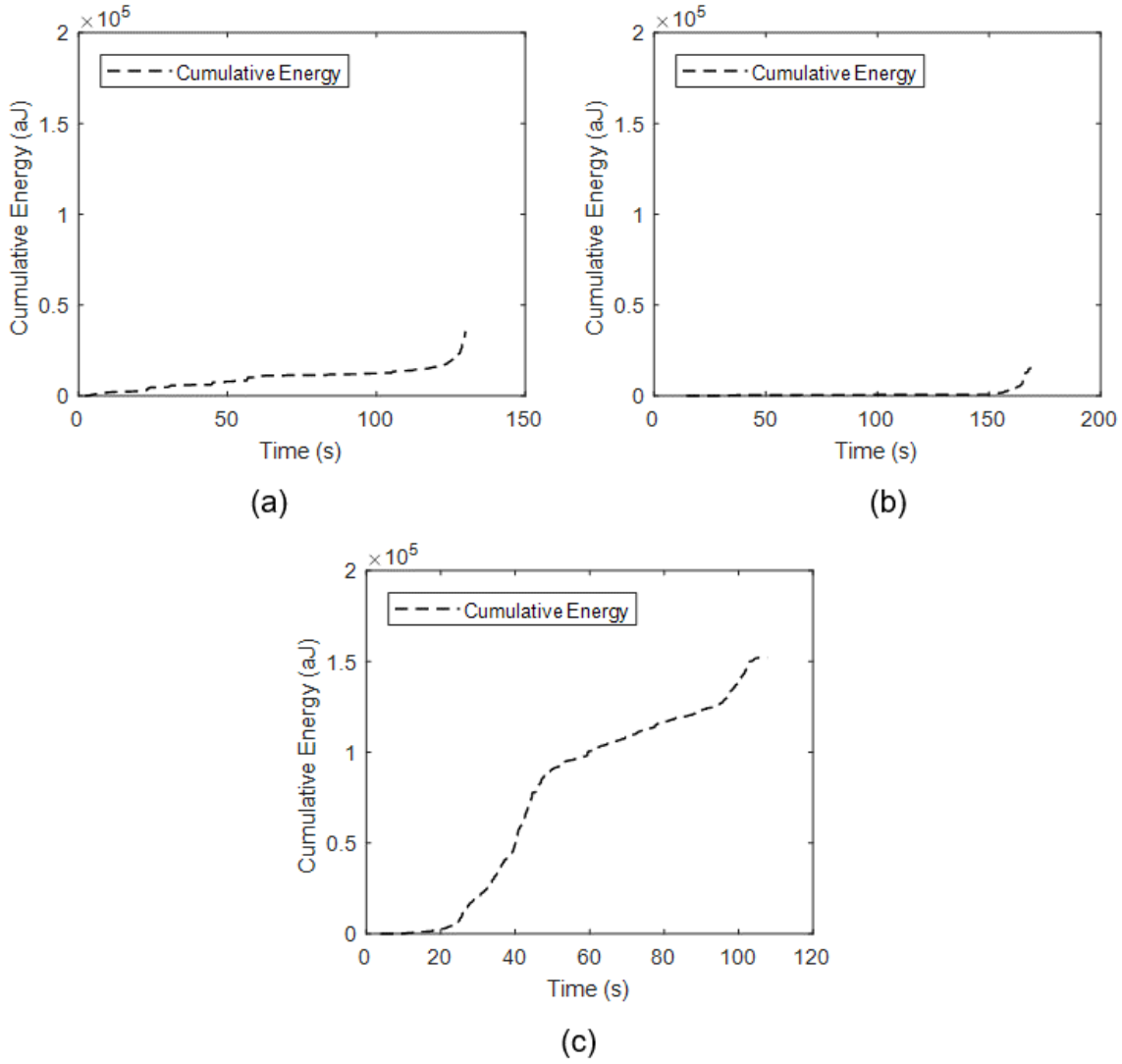

Figure 4-14: Cumulative energy with time for cylindrical specimens under cyclic wet-dry exposure regimen: (a) after 30-cycle; (b) after 60-cycle; (c) after 90-cycle

4.3.3.2 Cyclic Load Test - Cylindrical Specimen

In comparison to that previously observed for the cylindrical samples under cyclic step-loading, it would seem that the 30-cycle W-D sample may have had some level of damage as it indicated felicity effect for the low loading cycles (Figure 4-15a).

However, the recorded hits were low in energy and did not contribute significantly to increasing the cumulative energy (4-16a). These finding support that observed during the destructive study where the drop in compressive strength observed was deemed significant.

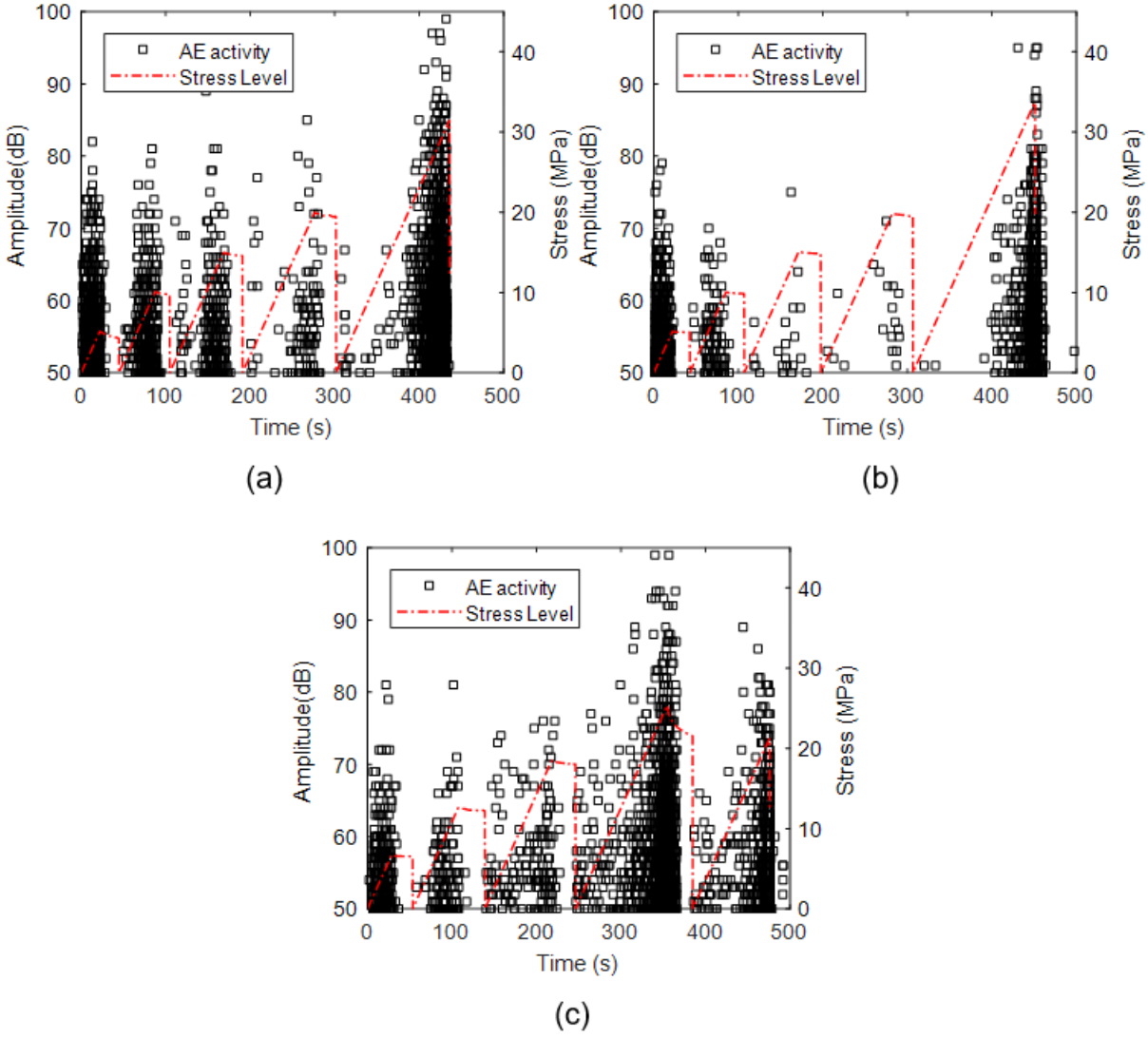

Figure 4-15: Acoustic emission activity and stress history with time for cylindrical specimens under cyclic wet-dry exposure regimen: (a) after 30-cycle; (b) after 60-cycle; (c) after 90-cycle

For the sample exposed to 90 W-D cycles (Figure 4-16c), the cylinder demonstrated signs of failure after the forth load cycle. There is a noticeable peak of high amplitude

hits with a rapid increase in cumulative energy reminiscent of macrocrack growth. For the fifth loading cycles, the sample actually failed at a lower load than its previous. Therefore, the fourth cycle was the actual ultimate loading peak. Here, the AE trend does not follow that previously seen and the differences between all three exposure levels cannot necessarily be differentiated with certainly.

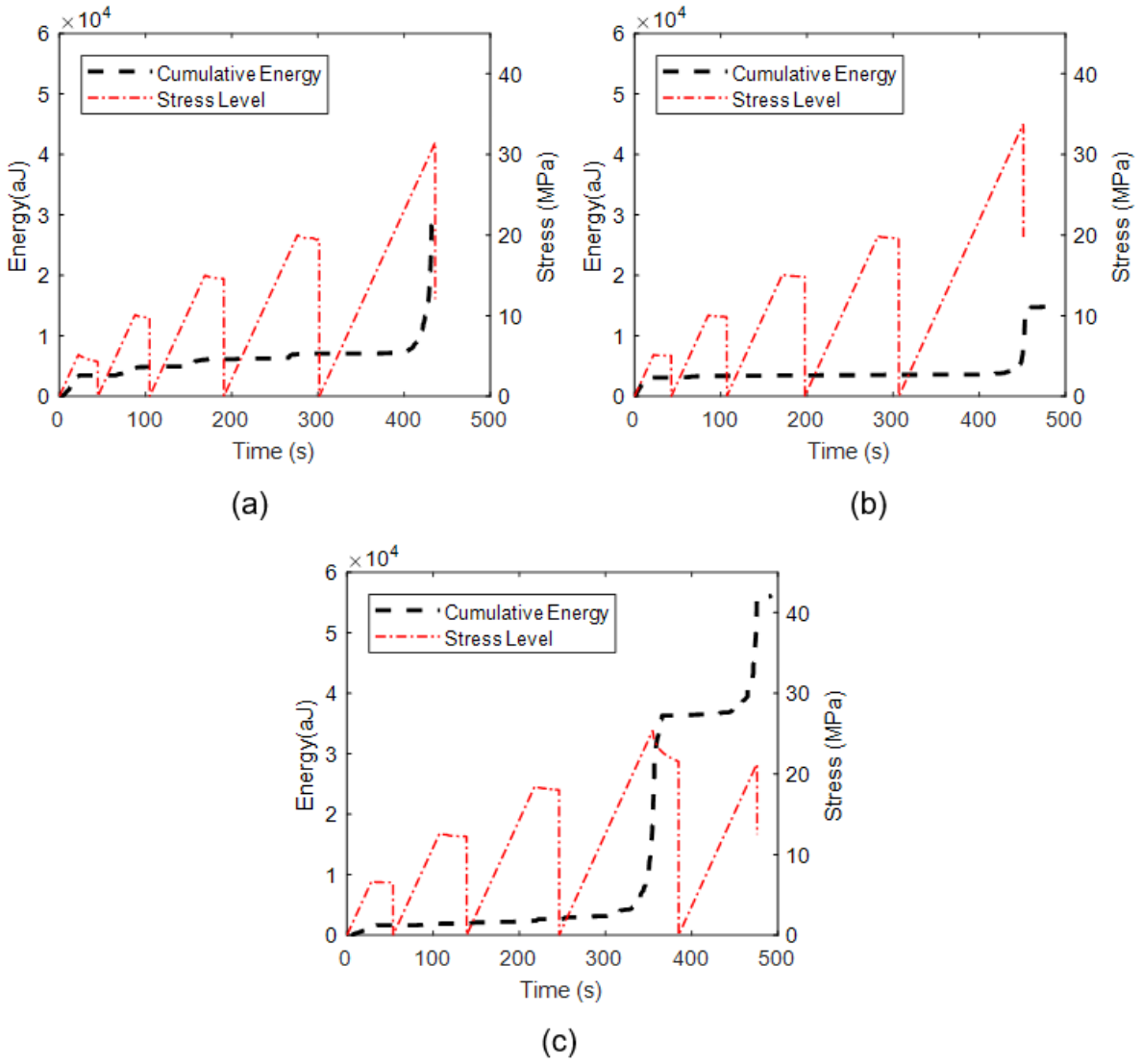

Figure 4-16: Cumulative energy with time for cylindrical specimens under cyclic wet-dry exposure regimen: (a) after 30-cycle; (b) after 60-cycle; (c) after 90-cycle

4.3.3.3 Monotonic Load Test - Prism Specimen

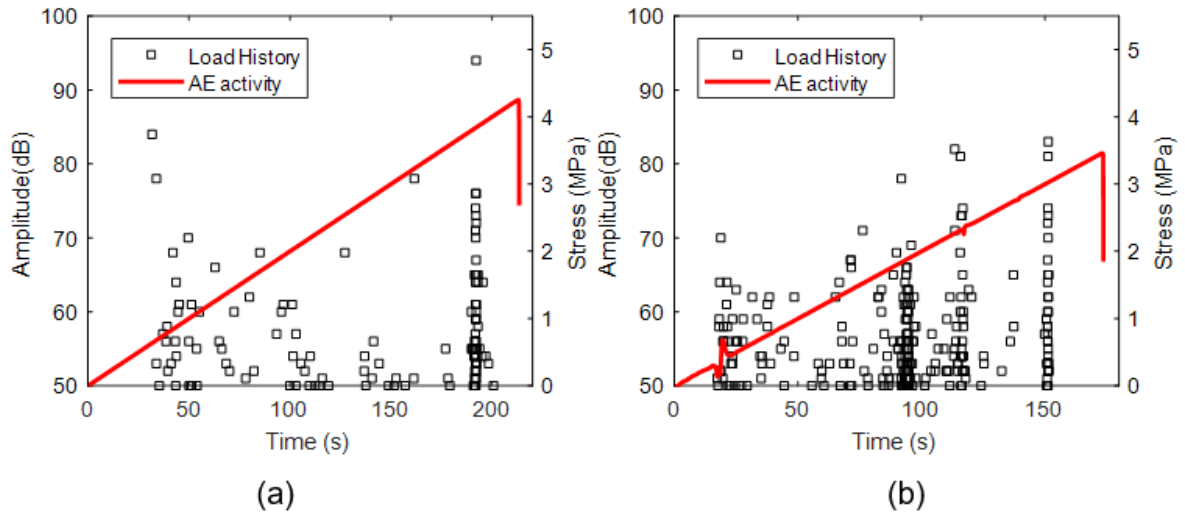

Figure 4-17: Acoustic emission activity and stress history with time for prism specimens under cyclic wet-dry exposure regimen: (a) after 30-cycle; (b) after 90-cycle

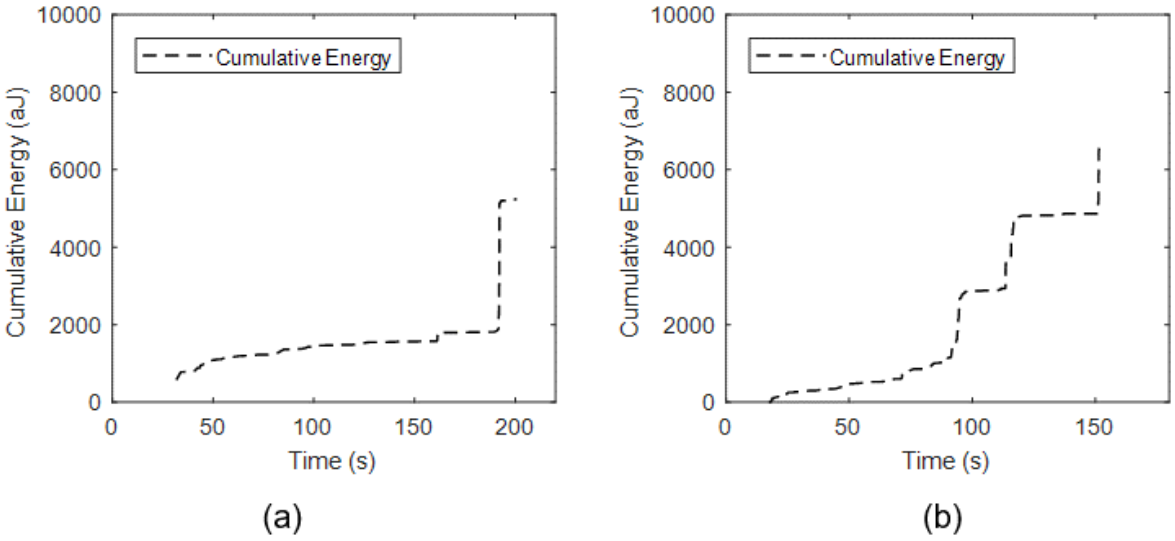

Figure 4-18: Cumulative energy with time for prism specimens under cyclic wet-dry exposure regimen: (a) after 30-cycle; (b) after 90-cycle

First, it needs to be mentioned that there are no results for the 60-cycle W-D exposure due to experimental error. Figures 4.17 and 4.18 show the results obtained for the acoustic emission monitoring during monotonic flexural loading of the 30-cycle and 90-

cycle W-D exposures only. The level in emissivity is quite low for both exposures. This corroborates that found previously where the 13.8% drop in strength was considered to be insignificant. Moreover, the cumulative energy (approximately 6000 aJ) is of the lowest recorded for this study.

4.3.3.4 Cyclic Load Test - Prism Specimen

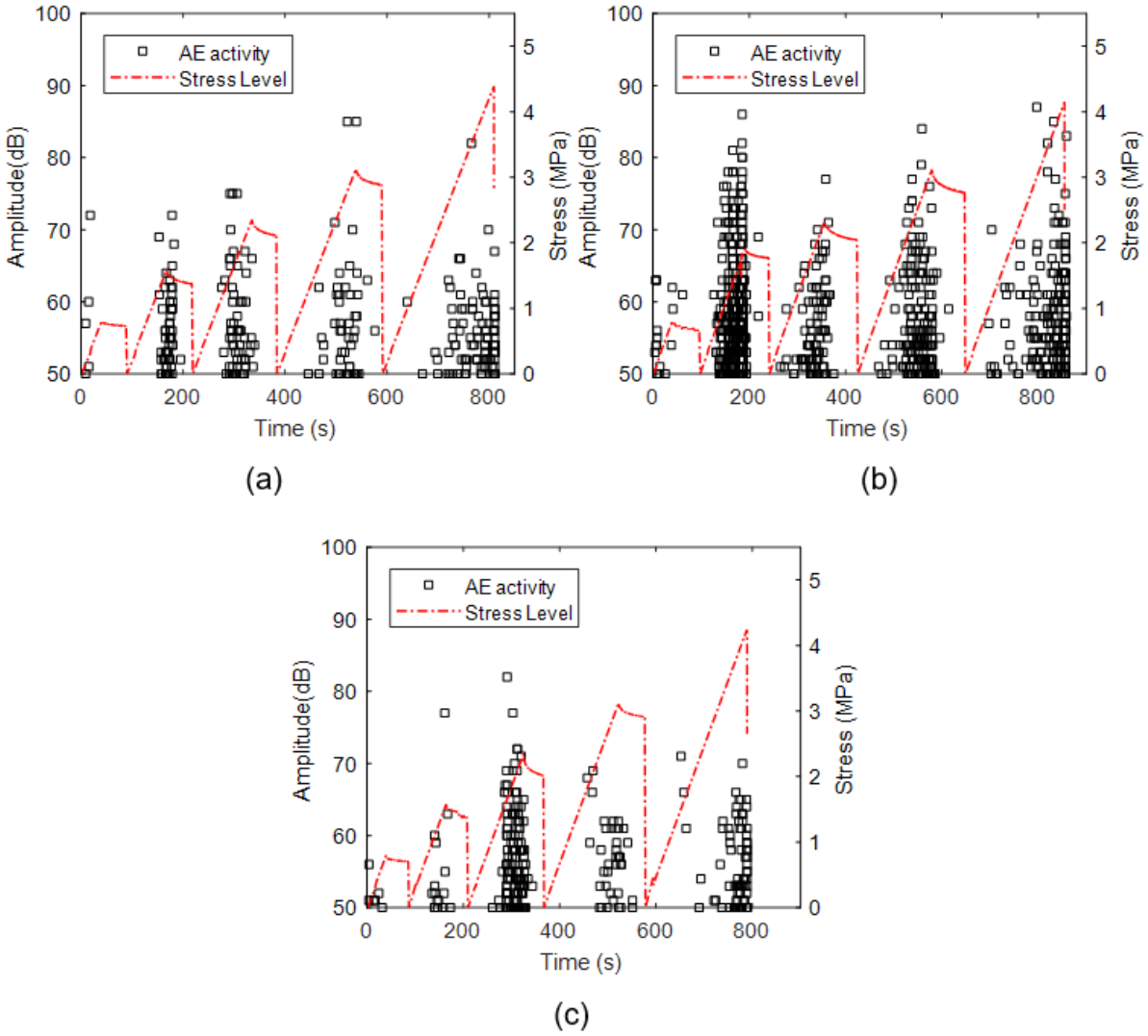

Figure 4-19: Acoustic emission activity and stress history with time for prism specimens under cyclic wet-dry exposure regimen: (a) after 30-cycle; (b) after 60-cycle; (c) after 90-cycle

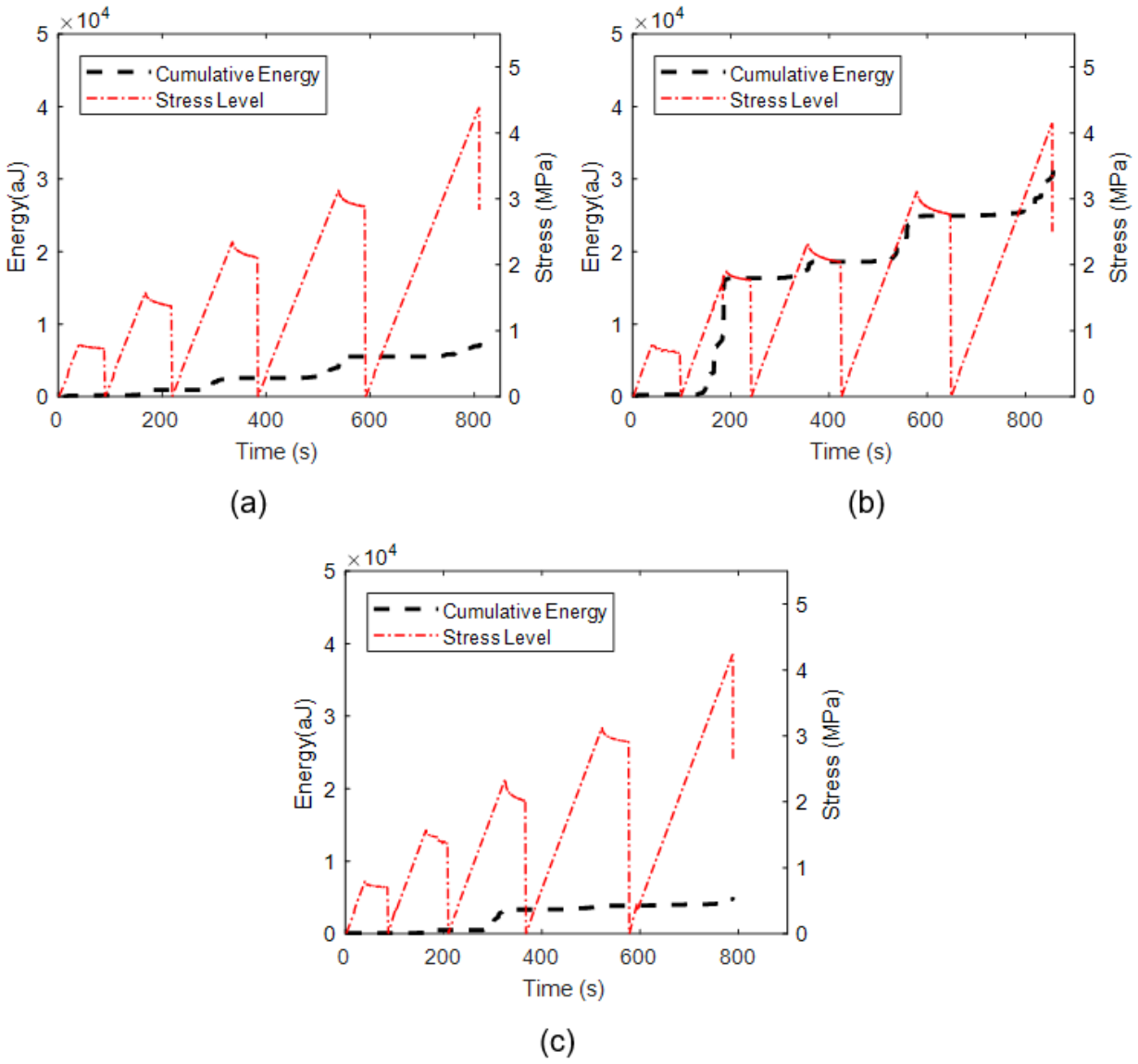

Figure 4-20: Cumulative energy with time for prism specimens under cyclic wet-dry exposure regimen: (a) after 30-cycle; (b) after 60-cycle; (c) after 90-cycle

Again, the same trend in results is reflected for the prism samples cyclically loaded. Here, the sample exposed to 60 wetting and drying cycles recorded the greatest number of hits with a higher level of cumulative energy. Interestingly, the trend of gain in cumulative energies follows a step pattern for each load cycles. It would seem that there is a felicity effect present (Figure 4-19b) were low energy emissions are recorded before the previous load level is reached. Thereafter, the hits recorded are of high energy contributing to the gains noticed in (Figure 4-20b). Once the load is released,

there are no emissions upon unloading. This is not the case for the 90-cycle specimen.

Seen in Figure 4-19c, the 90-cycle W-D specimen exhibits an increased number of hits during the third load cycles (60% of ultimate stress). This is accompanied with a gain in cumulative energy. Thereafter, there are very few emissions up to failure. Actually, emissions were recorded upon unloading during the fourth cycle which may be a sign of present damage to the sample affecting its integrity. It needs to be mentioned that this sample recorded the lowest dynamic modulus of elasticity which was substantially different from the other regimens types. Also, the 13.8% loss in flexural strength may have been significant if it had not been of the high coefficient of variation obtained (10%).

CONCLUSION

Based on the results of compressive strength alone presented in section 4.1, cyclic freezing and thawing may have caused an early onset of damage that may not have cumulated with growing number of cycles. As for cyclic high-temperature and wet-dry exposure regimens, damage progression mainly occurred in the third cyclic exposure as results demonstrated significant change after 90 cycles. However, this trend could not be confirmed for prismatic samples as results of flexural testing were inconclusive. Based on the results obtained for the destructive testing study, it would seem that these regimen types may not have caused a significant extent of damage due to the imposed temperature and moisture gradients. Perhaps a different test method may be more sensitive to assessing early onset of microstructural changes within the concrete matrix.

As previously mentioned in section 4.2, it would seem that nondestructive testing may better assess microstructural damage caused by the development of internal stresses. Here, resonant frequency seemed to be more effective than ultrasonic pulse velocity to discern the presence of microcracks in the material. This fact may be attributed to the frequency of the emitted pulse used in this study, 54 kHz. The use of a lower wave frequency means a higher pulse wavelength thus, less interaction with the bulk material. Here, the use of a higher pulse frequency (150 kHz and above) could have been more sensitive to micro-damage as the transient wave interacts with more material along its travel path. Still, the results of the study provide evidence that the exposure regimens did alter the mechanical properties of the concrete mixture evaluated.

To evaluate the residual performance of the material under load, acoustic emission monitoring was performed while loading to failure the specimens exposed to the various regimens. The trends in emissivity observed during both monotonic and cyclic loading confirmed that obtained for both the destructive and non-destructive testing. A simple analysis of recorded hits and cumulative energy versus applied stress was sufficient to

discern the presence of damage leading to a significant drop in mechanical properties for all three regimens replicated.

The nondestructive tools utilized in this study to evaluate damage induced by weathering conditions were successful. With proper test program configuration, ultrasonic testing and acoustic emission monitoring can be used in the field to assess the degree in damage along with monitoring its progression. Resonant frequency testing may be more appropriate for laboratory assessment.

Interestingly, the performance of a concrete material to resist the effects of cyclic high temperature exposure and moisture gradients are not commonly considered when designing a concrete mixture. Generally, freeze-thaw performance is the only weathering performance parameter considered. As such, further investigation is recommended to better understand the long-term effects of high temperature exposure and moisture gradients on concrete durability.

REFERENCES

[1] Neville, A. M. (1996). Properties of Concrete, 4th Ed., Pearson Education Ltd, 844 p.

[2] Lichtenstein, A. (1993). The Silver Bridge Collapse Recounted. Journal of Performance of Constructed Facilities, 7(4), 249-261.

[3] Fu, G. (2005). Inspection and monitoring techniques for bridges and civil structures. England: Woodhead Publishing Limited.

[4] Ryan, T. W., Mann, J. E., Chill, Z. M., & Ott, B. T. (2002). Bridge Inspector's Reference Manual (FHWA NHI 12-049).

[5] AASHTO. The Manual for Bridge Evaluation, 2nd Edition. Washington, D.C.: American Association of State Highway and Transportation Officials, 2008

[6] 364.1 R-07 - Guide for Evaluation of Concrete Structures Prior to Rehabilitation, ACI Committee 364, American Concrete Institute. Farmigton Hills, MI, 2007, 22 p.

[7] Bungey, J. H., Millard, S. G., Grantham, M. G. (2006). Testing of Concrete in Structures, 4th Ed., Taylor and Francis, New York, NY, 339 p.

[8] Eisenblätter, J., Grosse, C. U., Köppel, S., Kurz, J. H., Landis, E. N., Linzer, L. M., Vogel, T. (2008). Acoustic Emission Testing: Basic for Research-Applications in Civil Engineering. Eds C. U. Grosse & M. Ohtsu, Berlin, Germany: Springer.

[9] Kaiser, J. (1950). A study of acoustic phenomena in tensile tests. Ph.D. dissertation, Technical University of Munich

[10] Kawasaki, Y., Wakuda, T., Kobarai, T., & Ohtsu, M. (2013). Corrosion mechanisms in reinforced concrete by acoustic emission. Construction and Building Materials, 48, 1240-1247.

[11] Abdelrahman, M., ElBatanouny, M. K., Ziehl, P., Fasl, J., Larosche, C. J., & Fraczek, J. (2015). Classification of alkali–silica reaction damage using acoustic emission: A proof-of-concept study. Construction and Building Materials, 95, 406-413.

[12] Qian, Y., Farnam, Y., & Weiss, J. (2014). Using Acoustic Emission to Quantify Freeze–Thaw Damage of Mortar Saturated with NaCl Solutions. Proceedings of the 4th International Conference on the Durability of Concrete Structures.

[13] Huang M, Jiang L, Liaw P. K, Brooks C. R, Seeley R, Klarstrom D. L. (1998). Using acoustic emission in fatigue and fracture materials research. Journal of the Minerals, Metals and Materials Society, 50 (11).

[14] Mindess, S. (2004). Acoustic Emission Methods, Handbook on Nondestructive Testing of Concrete. Ed. V.M. Malhotra and N.J. Carino, 2nd Edition, CRC Press, Chap. 16.

[15] ASTM Standard E1316 (2017a). Standard Terminology for Nondestructive Examinations, ASTM International, West Conshohocken, PA.

[16] Behnia, A., Chai, H. K., & Shiotani, T. (2014). Advanced structural health monitoring of concrete structures with the aid of acoustic emission. Construction and Building Materials, 65, 282-302.

[17] ASTM C215 (2014). Standard Test Method for Fundamental Transverse, Longitudinal, and Torsional Resonant Frequencies of Concrete Specimens, ASTM International, West Conshohocken, PA.

[18] ASTM Standard C597 (2014). Standard Test Method for Pulse Velocity Through Concrete," ASTM International, West Conshohocken, PA.

[19] ASTM C39 (2016). Standard Test Method for Compressive Strength of Cylindrical Concrete Specimens, ASTM International, West Conshohocken, PA

[20] ASTM C78 (2015b), Standard Test Method for Flexural Strength of Concrete (Using Simple Beam with Third-Point Loading), ASTM International, West Conshohocken, PA.

[21] ASTM E2374 (2016). Standard Guide for Acoustic Emission System Performance Verification, ASTM International, West Conshohocken, PA

[22] Boyd, Andrew. J. and Christopher C. Ferraro (2005). Effect of Curing and Deterioration on Stress Wave Velocities in Concrete. Journal of Material in Civil Engineering, 17, 2, 153-158.

[23] Hartell J., Boyd A. J., Rivard P. (2017) Efficacy of Ultrasonic Pulse Velocity Testing to Assess Sulfate-Degraded Concrete, Sulfate Attack on Concrete: A Holistic Perspective, ACI Special Publication.